

# High-order, linearly stable, partitioned solvers for general multiphysics problems based on implicit-explicit Runge-Kutta schemes

D. Z. Huang<sup>a,1,\*</sup>, P.-O. Persson<sup>b,c,2</sup>, M. J. Zahr<sup>b,d,3,4,\*</sup>

<sup>a</sup>*Institute for Computational and Mathematical Engineering, Stanford University, Stanford, CA, 94305, United States*

<sup>b</sup>*Mathematics Group, Lawrence Berkeley National Laboratory, 1 Cyclotron Road, Berkeley, CA 94720, United States*

<sup>c</sup>*Department of Mathematics, University of California, Berkeley, Berkeley, CA 94720, United States*

<sup>d</sup>*Department of Aerospace and Mechanical Engineering, University of Notre Dame, Notre Dame, IN, 46556, United States*

## Abstract

This work introduces a general framework for constructing high-order, linearly stable, partitioned solvers for multiphysics problems from a monolithic implicit-explicit Runge-Kutta (IMEX-RK) discretization of the semi-discrete equations. The generic multiphysics problem is modeled as a system of  $n$  systems of partial differential equations where the  $i$ th subsystem is coupled to the other subsystems through a coupling term that can depend on the state of all the other subsystems. This coupled system of partial differential equations reduces to a coupled system of ordinary differential equations via the method of lines where an appropriate spatial discretization is applied to each subsystem. The coupled system of ordinary differential equations is taken as a monolithic system and discretized using an IMEX-RK discretization with a specific implicit-explicit decomposition that introduces the concept of a *predictor* for the coupling term. We propose four coupling predictors that enable the monolithic system to be solved in a partitioned manner, i.e., subsystem-by-subsystem, and preserve the IMEX-RK structure and therefore the design order of accuracy of the monolithic scheme. The four partitioned solvers that result from these predictors are high-order accurate, allow for maximum re-use of existing single-physics software, and two of the four solvers allow the subsystems to be solved in parallel at a given stage and time step. We also analyze the stability of a coupled, linear model problem with a specific coupling structure and show that one of the partitioned solvers achieves unconditional linear stability for this problem, while the others are unconditionally stable only for certain values of the coupling strength. We demonstrate the performance of the proposed partitioned solvers on several classes of multiphysics problems including a simple linear system of ODEs, advection-diffusion-reaction systems, fluid-structure interaction problems, and particle-laden flows, where we verify the design order of the IMEX schemes and study various stability properties.

## 1. Introduction

The numerical simulation of multiphysics problems involving multiple physical models or multiple simultaneous physical phenomena is significant in many engineering and scientific applications, e.g., aircraft flutter in transonic flows [1], biomedical flows in heart and blood vessels [2], mixing and chemically reacting flows [3], reactor fuel performance [4], turbomachinery [5], magnetohydrodynamics [6] and so on. These problems are generally highly nonlinear, feature multiple scales and strong coupling effects, and require heterogeneous discretizations for the various physics subsystems. To balance the treatment of these features, solution strategies ranging from a monolithic approach to partitioned procedures have been proposed.

In the monolithic approach [7, 8, 9], all physical subsystems are solved simultaneously and is therefore preferred in the case of strong interactions to ensure stability. However, when the coupled subsystems

---

\*Corresponding author

<sup>1</sup>Graduate Student, Institute for Computational and Mathematical Engineering, Stanford University

<sup>2</sup>Associate Professor, Department of Mathematics, University of California, Berkeley

<sup>3</sup>Luis W. Alvarez Postdoctoral Fellow, Computational Research Division, Lawrence Berkeley National Laboratory

<sup>4</sup>Assistant Professor, Department of Aerospace and Mechanical Engineering, University of Notre Dame

are complex, the monolithic procedure can be suboptimal and often requires significant implementation effort since only small components of existing software can be re-used. An alternative is the partitioned procedure [10, 11, 12], also known as a staggered or a loosely coupled procedure, where different subsystems are modeled and discretized separately, and the resulting equations are solved independently. The coupling occurs through specific terms that are lagged to previous time instances and communicated between solvers. This procedure facilitates software modularity and mathematical modeling; however, these schemes are often low-order accurate [11] (second order accuracy) and suffer from lack of stability [13].

Recently, a partitioned solver based on implicit-explicit Runge-Kutta schemes, first proposed to solve stiff additive ordinary differential equations [14, 15], was proposed [16, 17] in the context of a specific multiphysics system: fluid-structure interaction. This solver demonstrated up to fifth-order accuracy without requiring the solution of the fully coupled fluid-structure system. A key feature of this solver that distinguishes it from other work on IMEX-RK methods for multiphysics systems [18] is that both the fluid and the structure subsystems are handled implicitly and only a correction to the predicted traction on the structure is treated explicitly. Therefore the stability of this IMEX-RK partitioned procedure is expected to be better than explicit schemes and nearly as good as fully implicit schemes. Despite the advantages of the partitioned fluid-structure interaction solver in [16, 17], it is not directly applicable to other multiphysics systems and their proposed traction predictor combines stage information in a heuristic way, which may lead to accuracy reduction.

Inspired by these works, we built a general framework to construct high-order partitioned solvers based on monolithic IMEX-RK discretizations for general multiphysics systems. We consider a general model of multiphysics problems as a system of  $n$  systems of partial differential equations, coupled through specific coupling terms that can depend on the state of all physical subsystems, and which is reduced to a system of ODEs after semi-discretization. An IMEX-RK discretization is applied to this monolithic system of ODEs, with a specific implicit-explicit decomposition that introduces the concept of a predictor. The implicit part of the decomposition is taken as the entire multiphysics system where the coupling term is replaced by the predictor and the explicit part is a correction to the system that accounts for errors in the coupling predictor. Predictors that satisfy basic properties outlined in this work will allow the monolithic discretization to be solved in a partitioned manner, i.e., subsystem-by-subsystem. Four consistent predictors are introduced, including weak and strong Jacobi-type predictors and weak and strong Gauss-Seidel-type predictors, that lead to different partitioned solvers that maintain the design order of accuracy of the IMEX-RK scheme. However, the solvers resulting from these four predictors have their own strengths and limitations by trading off between implementation effort, stability, and efficiency. The weak predictors require the least implementation effort since they do not require any terms from the Jacobian of the coupling term, while the strong predictors require the diagonal entries. The Jacobi predictors allow for system-wise parallelization, while the Gauss-Seidel predictors require the subsystems be solved sequentially. Despite the simplicity and efficiency of the weak and the Jacobi predictors over the strong and the Gauss-Seidel predictors, they have weaker linear stability properties, which we demonstrate through linear stability analysis of the four predictors applied to a chosen linear model problem and provide numerical evidence. It is worth noting that, through our linear stability analysis, we find the strong Gauss-Seidel predictor leads to an unconditionally stable scheme when applied to the chosen model problem, despite being a partitioned solver. The splitting choice implied by the strong Gauss-Seidel predictor minimizes the explicit contribution to the scheme and, in many cases, the implicit part appears to stabilize growing modes produced by the explicit part. Finally, we note that given the generality of this formulation, the proposed solver can be applied to a vast number of multiphysics problems; however, it is well-known that partitioned solvers are unstable for certain physical regimes, including fluid-structure interaction at low mass ratios and magnetohydrodynamics with strong bidirectional coupling, which is not included by our linear stability analysis. We include a more general stability analysis to show the physical regimes, i.e., coupling strength, in which the strong Gauss-Seidel predictor is unconditionally stable.

The remainder of the paper is organized as follows. In Section 2, the general form of the multiphysics problem as a system of  $n$  systems of partial differential equations and its semi-discretization are introduced. In Section 3, an overview of IMEX-RK schemes is provided and a specific implicit-explicit decomposition

using the concept of a coupling predictor is introduced. Additionally, four predictors are introduced that lead to different solvers and their features such as accuracy, implementation effort, efficiency, and stability are discussed. A slew of applications are provided in Sections 4-7 that demonstrate the high-order accuracy, stability, and robustness of the proposed solvers on an advection-diffusion-reaction system, fluid-structure interaction problems, and particle-laden flows.

## 2. Governing multiphysics equations and semi-discretization

Consider a general formulation of a mathematical model describing the behavior of multiple interacting physical phenomena described by the following coupled system of partial differential equations

$$\partial_t u^i = \mathcal{L}^i(u^i, \mathbf{c}^i, x, t), \quad x \in \Omega^i(\mathbf{c}^i), \quad t \in (0, T) \quad (1)$$

for  $i = 1, \dots, m$ , where  $m$  represents the number of physical systems, and boundary conditions are excluded for brevity. The  $i$ th physical system is modeled as a partial differential equation characterized by the generalized differential operator  $\mathcal{L}^i$  that defines a conservation law or other type of balance law, the state variable  $u^i(x, t)$  that is the solution of the  $i$ th physical system on the space-time domain  $\Omega^i \times (0, T)$ , and a *coupling term*  $\mathbf{c}^i$  that, in general, couples the  $i$ th system to the other  $m - 1$  systems. In the general case, the differential operator  $\mathcal{L}^i$ , domain  $\Omega^i$ , and boundary conditions depend on the coupling term. The coupling term contains quantities usually considered *data* required to define the  $i$ th PDE, such as boundary conditions or material properties. In a single-physics setting, these quantities would be prescribed, but in the multiphysics setting they are determined from the state vectors of all  $m$  systems, i.e.,

$$\mathbf{c}^i = \mathbf{c}^i(u^1, \dots, u^m, x, t). \quad (2)$$

The definition of the coupling term is problem-dependent and it will be shown that special structure in the coupling term can be exploited to create a better partitioned solver. While the form of (1) is specific to first-order temporal systems, it includes equations with higher-order temporal derivatives, assuming they have been re-cast in first-order form. The spatial domains  $\Omega^i$  for the individual systems may or may not be overlapping and in many cases are the same, i.e.,  $\Omega^i = \Omega$  for  $i = 1, \dots, m$ .

As this work is focused on the development of high-order partitioned schemes for evolving multiphysics problems, we introduce the semi-discrete form of the coupled partial differential equations in (1) that arises from applying an appropriate spatial discretization to the  $i$ th PDE system individually, which takes the form

$$\mathbf{M}^i \dot{\mathbf{u}}^i = \mathbf{r}^i(\mathbf{u}^i, \mathbf{c}^i, t), \quad t \in (0, T) \quad (3)$$

where  $\mathbf{u}^i(t)$  is the semi-discrete state vector corresponding to the spatial discretization of  $u^i(x, t)$ ,  $\mathbf{r}^i$  is the spatial discretization of the differential operator  $\mathcal{L}^i$  and called the velocity of the ODE system in the remainder of the document, and  $\mathbf{c}^i$  is the semi-discrete coupling term corresponding to the spatial discretization of  $\mathbf{c}^i(u^1, \dots, u^m, x, t)$ . In general, the coupling term depends on the semi-discrete state vector of all  $m$  systems

$$\mathbf{c}^i = \mathbf{c}^i(\mathbf{u}^1, \dots, \mathbf{u}^m, t). \quad (4)$$

For convenience, we re-write the system of ordinary differential equations in (3)-(4) as

$$\mathbf{M} \dot{\mathbf{u}} = \mathbf{r}(\mathbf{u}, \mathbf{c}(\mathbf{u}, t), t), \quad t \in (0, T), \quad (5)$$

where the combined mass matrix is a block diagonal matrix consisting of the single-physics mass matrices

$$\mathbf{M} = \begin{bmatrix} \mathbf{M}^1 & & \\ & \ddots & \\ & & \mathbf{M}^m \end{bmatrix} \quad (6)$$

and the combined state vector, coupling term, and nonlinear residual are vectors consisting of the corresponding single-physics term, concatenated across all  $m$  systems

$$\mathbf{u} = \begin{bmatrix} \mathbf{u}^1 \\ \vdots \\ \mathbf{u}^m \end{bmatrix} \quad \mathbf{c}(\mathbf{u}, t) = \begin{bmatrix} \mathbf{c}^1(\mathbf{u}^1, \dots, \mathbf{u}^m, t) \\ \vdots \\ \mathbf{c}^m(\mathbf{u}^1, \dots, \mathbf{u}^m, t) \end{bmatrix} \quad \mathbf{r}(\mathbf{u}, \mathbf{c}, t) = \begin{bmatrix} \mathbf{r}^1(\mathbf{u}^1, \mathbf{c}^1, t) \\ \vdots \\ \mathbf{r}^m(\mathbf{u}^m, \mathbf{c}^m, t) \end{bmatrix}. \quad (7)$$

The total derivative, or Jacobian, of the semi-discrete velocity  $D_{\mathbf{u}}\mathbf{r}$  is expanded as

$$D_{\mathbf{u}}\mathbf{r} = \frac{\partial \mathbf{r}}{\partial \mathbf{u}} + \frac{\partial \mathbf{r}}{\partial \mathbf{c}} \frac{\partial \mathbf{c}}{\partial \mathbf{u}}, \quad (8)$$

where the individual terms take the form

$$\frac{\partial \mathbf{r}}{\partial \mathbf{u}} = \begin{bmatrix} \frac{\partial \mathbf{r}^1}{\partial \mathbf{u}^1} & & \\ & \ddots & \\ & & \frac{\partial \mathbf{r}^m}{\partial \mathbf{u}^m} \end{bmatrix} \quad \frac{\partial \mathbf{r}}{\partial \mathbf{c}} = \begin{bmatrix} \frac{\partial \mathbf{r}^1}{\partial \mathbf{c}^1} & & \\ & \ddots & \\ & & \frac{\partial \mathbf{r}^m}{\partial \mathbf{c}^m} \end{bmatrix} \quad \frac{\partial \mathbf{c}}{\partial \mathbf{u}} = \begin{bmatrix} \frac{\partial \mathbf{c}^1}{\partial \mathbf{u}^1} & \dots & \frac{\partial \mathbf{c}^1}{\partial \mathbf{u}^m} \\ \vdots & \ddots & \vdots \\ \frac{\partial \mathbf{c}^m}{\partial \mathbf{u}^1} & \dots & \frac{\partial \mathbf{c}^m}{\partial \mathbf{u}^m} \end{bmatrix}, \quad (9)$$

and the dependencies have been dropped for brevity. The first term in the Jacobian is block diagonal and accounts for the direct contribution of a state to its own system while the second term accounts for the coupling between systems. Several examples of this general multiphysics formulation are provided in Sections 5-7 including advection-diffusion-reaction systems, two-field and three-field fluid-structure interaction problems, and particle-laden flows. The semi-discrete forms of the multiphysics problem in (3) and (5) will be the point of departure for the remainder of this document and the starting point for the introduction of our proposed high-order partitioned solvers.

### 3. A high-order partitioned solver for multiphysics problems

In this section, we introduce our proposed high-order partitioned time-integration scheme for multiphysics systems. As discussed in Section 1, a partitioned solver combines individual, single-physics solvers into an integration scheme for the multiphysics problem, rather than considering the monolithic multiphysics system. A partitioned solver can reduce computational complexity per time-step, improve software maintainability, and exploit off-the-shelf software components; however they tend to be limited to low-order accuracy and have stringent stability requirements. Our partitioned time-integration scheme mitigates most of these issues by combining high-order implicit-explicit Runge-Kutta (IMEX) schemes for the monolithic multiphysics system with a judicious implicit-explicit decomposition that partially decouples the individual systems via a novel predictor for the coupling terms.

#### 3.1. Background: implicit-explicit Runge-Kutta schemes

Implicit-explicit Runge-Kutta schemes, first proposed in [14, 15], define a family of high-order discretizations for nonlinear differential equations whose velocity term can be decomposed into a sum of a non-stiff  $\mathbf{f}$  and stiff  $\mathbf{g}$  velocity

$$M\dot{\mathbf{u}} = \mathbf{f}(\mathbf{u}, t) + \mathbf{g}(\mathbf{u}, t). \quad (10)$$

The non-stiff  $\mathbf{f}$  velocity is integrated with an  $s$ -stage explicit Runge-Kutta scheme and the stiff term  $\mathbf{g}$  is integrated with an  $s$ -stage diagonally implicit Runge-Kutta scheme. IMEX Runge-Kutta schemes are compactly represented by a double tableau in the usual Butcher notation (Table 1), where  $\hat{A}$ ,  $\hat{b}$ ,  $\hat{c}$  defines the Butcher tableau for the explicit Runge-Kutta scheme used for  $\mathbf{f}$  and  $A$ ,  $b$ ,  $c$  defines the diagonally implicit Runge-Kutta scheme used for  $\mathbf{g}$ . In this work, we mainly consider 2nd-order 2-stage trapezoidal rule, 3rd-order 4-stage ARK3(2)4L[2]SA, and 4th-order 6 stage ARK4(3)6L[2]SA proposed in [19]. Theoretically, IMEX schemes can be of arbitrarily high order accuracy, but as the number of stages increases, inexactness

of the coefficients may destroy the order of accuracy. The implicit Runge-Kutta part of these IMEX schemes are L-stable, stiffly-accurate, and have an explicit first stage ( $a_{11} = 0$ ).

Explicit Runge-Kutta coefficients	Implicit Runge-Kutta coefficients
$\begin{array}{c cccc} 0 & & & & \\ \hat{c}_2 & \hat{a}_{21} & & & \\ \hat{c}_3 & \hat{a}_{31} & \hat{a}_{32} & & \\ \vdots & \vdots & & \ddots & \\ \hat{c}_s & \hat{a}_{s1} & a_{s2} & \cdots & \hat{a}_{ss-1} \\ \hline & \hat{b}_1 & \hat{b}_2 & \cdots & \hat{b}_{s-1} & \hat{b}_s \end{array}$	$\begin{array}{c cccccc} c_1 & & & & & \\ c_2 & a_{21} & a_{22} & & & \\ c_3 & a_{31} & a_{32} & a_{33} & & \\ \vdots & \vdots & & & \ddots & \\ c_s & a_{s1} & a_{s2} & \cdots & a_{ss-1} & a_{ss} \\ \hline & b_1 & b_2 & \cdots & b_{s-1} & b_s \end{array}$

Table 1: Butcher Tableau for s-stage implicit-explicit Runge-Kutta scheme

Consider a discretization of the time domain  $[0, T]$  into  $N_t$  segments with endpoints  $\{t_0, \dots, t_{N_t}\}$ , with the  $n$ th segment having length  $\Delta t_n = t_n - t_{n-1}$  for  $n = 1, \dots, N_t$ . Also, let  $\mathbf{u}_n$  denote the approximation of the solution of the differential equation in (10) at time step  $n$ , i.e.,  $\mathbf{u}_n \approx \mathbf{u}(t_n)$ . Then, given the explicit  $(\hat{A}, \hat{b}, \hat{c})$  and implicit  $(A, b, c)$  Butcher tableaus, the  $s$ -stage IMEX Runge-Kutta scheme that advances  $\mathbf{u}_{n-1}$  to  $\mathbf{u}_n$  is given by

$$\mathbf{u}_n = \mathbf{u}_{n-1} + \sum_{p=1}^s \hat{b}_p \hat{\mathbf{k}}_{n,p} + \sum_{p=1}^s b_p \mathbf{k}_{n,p}, \quad (11a)$$

$$\mathbf{M}\mathbf{k}_{n,j} = \Delta t_n \mathbf{g}(\mathbf{u}_{n,j}, t_{n-1} + c_j \Delta t_n), \quad (11b)$$

$$\mathbf{M}\hat{\mathbf{k}}_{n,j} = \Delta t_n \mathbf{f}(\mathbf{u}_{n,j}, t_{n-1} + \hat{c}_j \Delta t_n), \quad (11c)$$

$$\mathbf{u}_{n,j} = \mathbf{u}_{n-1} + \sum_{p=1}^{j-1} \hat{a}_{jp} \hat{\mathbf{k}}_{n,p} + \sum_{p=1}^j a_{jp} \mathbf{k}_{n,p}, \quad (11d)$$

where  $\hat{\mathbf{k}}_{n,p}$  and  $\mathbf{k}_{n,p}$  are the  $p$ th explicit and implicit velocity stage, respectively, corresponding to time step  $n$  and  $\mathbf{u}_{n,p}$  is the approximation to  $\mathbf{u}_n$  at stage  $p$  of time step  $n$ . The complete algorithm to advance  $\mathbf{u}_{n-1}$  to  $\mathbf{u}_n$  using the IMEX Runge-Kutta scheme is provided in Algorithm 1. For each stage  $j$ , the nonlinear system of equations in (11b) must be solved to compute the implicit stage  $\mathbf{k}_{n,j}$ . Next, the explicit stage can be computed directly from (11c) since the stage approximation  $\mathbf{u}_{n,j}$  does not depend on the explicit stage  $\hat{\mathbf{k}}_{n,j}$ . Finally, given the previous time step and all implicit and explicit stages, the solution at time  $n$  is determined from (11a).

---

**Algorithm 1** Implicit-Explicit Runge-Kutta scheme

---

1: **for** stages  $j = 1, \dots, s$  **do**

2: Define stage solution according to (11a):  $\mathbf{u}_{n,j} = \mathbf{u}_{n-1} + \sum_{p=1}^{j-1} \hat{a}_{jp} \hat{\mathbf{k}}_{n,p} + \sum_{p=1}^j a_{jp} \mathbf{k}_{n,p}$

3: Implicit solve (11b) for  $\mathbf{k}_{n,j}$ :  $\mathbf{M}\mathbf{k}_{n,j} = \Delta t_n \mathbf{g}(\mathbf{u}_{n,j}, t_{n-1} + c_j \Delta t_n)$

4: Explicit solve (11c) for  $\hat{\mathbf{k}}_{n,j}$ :  $\mathbf{M}\hat{\mathbf{k}}_{n,j} = \Delta t_n \mathbf{f}(\mathbf{u}_{n,j}, t_{n-1} + \hat{c}_j \Delta t_n)$

5: **end for**

6: Set  $\mathbf{u}_n = \mathbf{u}_{n-1} + \sum_{p=1}^s \hat{b}_p \hat{\mathbf{k}}_{n,p} + \sum_{p=1}^s b_p \mathbf{k}_{n,p}$

---

### 3.2. A partitioned implicit-explicit Runge-Kutta scheme for multiphysics systems

The proposed high-order partitioned scheme for integration of generic time-dependent multiphysics problems of the form (3)-(4) is built on an IMEX Runge-Kutta discretization of the monolithic system. A special choice of implicit-explicit decomposition, along with the introduction of four predictors for the coupling term, creates a *diagonal* (uncoupled) or *triangular* dependency between the systems and allows the monolithic discretization to be solved in a partitioned manner. The proposed decomposition handles a majority of the relevant physics *implicitly* to leverage the enhanced stability properties of such schemes, while only the correction to the coupling predictor is handled explicitly. This marks a key difference to previous work on IMEX Runge-Kutta schemes for multiphysics systems [18] that choose the implicit-explicit splitting based on stiffness of the physics. It will be shown in Section 3.2.4 that the proposed predictors preserve the accuracy and stability properties of the IMEX scheme.

#### 3.2.1. Implicit-explicit decomposition and monolithic IMEX Runge-Kutta discretization

To begin our construction, recall the semi-discrete form of the multiphysics system (5) and consider the splitting of the velocity term  $\mathbf{r}(\mathbf{u}, \mathbf{c}(\mathbf{u}, t), t)$  as

$$\mathbf{r}(\mathbf{u}, \mathbf{c}(\mathbf{u}, t), t) = \mathbf{f}(\mathbf{u}, \tilde{\mathbf{c}}, t) + \mathbf{g}(\mathbf{u}, \tilde{\mathbf{c}}, t) \quad (12)$$

where  $\tilde{\mathbf{c}}$  is an approximation, or *predictor*, of the coupling term  $\mathbf{c}(\mathbf{u}, t)$  and the terms that will be handled explicitly  $\mathbf{f}$  and implicitly  $\mathbf{g}$  in the IMEX discretization are defined as

$$\mathbf{f}(\mathbf{u}, \tilde{\mathbf{c}}, t) = \mathbf{r}(\mathbf{u}, \mathbf{c}(\mathbf{u}, t), t) - \mathbf{r}(\mathbf{u}, \tilde{\mathbf{c}}, t) \quad (13a)$$

$$\mathbf{g}(\mathbf{u}, \tilde{\mathbf{c}}, t) = \mathbf{r}(\mathbf{u}, \tilde{\mathbf{c}}, t), \quad (13b)$$

where the dependence on the predictor is explicitly included. In general, the predictor depends on the instantaneous state vector  $\mathbf{u}(t)$  and data  $\bar{\mathbf{u}}$ , likely from the history of the state vector  $\{\mathbf{u}(\tau) \mid \tau < t\}$

$$\tilde{\mathbf{c}} = \tilde{\mathbf{c}}(\mathbf{u}, \bar{\mathbf{u}}, t). \quad (14)$$

With this decomposition of the velocity of the semi-discrete multiphysics system in (13), the IMEX Runge-Kutta scheme in (11) applied to the monolithic multiphysics system (5) becomes

$$\begin{aligned} \mathbf{u}_n &= \mathbf{u}_{n-1} + \sum_{p=1}^s \hat{b}_p \hat{\mathbf{k}}_{n,p} + \sum_{p=1}^s b_p \mathbf{k}_{n,p}, \\ \mathbf{M} \mathbf{k}_{n,j} &= \Delta t_n \mathbf{g}(\mathbf{u}_{n,j}, \tilde{\mathbf{c}}(\mathbf{u}_{n,j}, \mathbf{u}_{n-1}, t_{n,j}), t_{n,j}), \\ \mathbf{M} \hat{\mathbf{k}}_{n,j} &= \Delta t_n \mathbf{f}(\mathbf{u}_{n,j}, \tilde{\mathbf{c}}(\mathbf{u}_{n,j}, \mathbf{u}_{n-1}, t_{n,j}), t_{n,j}), \\ \mathbf{u}_{n,j} &= \mathbf{u}_{n-1} + \sum_{p=1}^{j-1} \hat{a}_{jp} \hat{\mathbf{k}}_{n,p} + \sum_{p=1}^j a_{jp} \mathbf{k}_{n,p}, \end{aligned} \quad (15)$$

where the data used in the coupling predictor is taken from the previous time step. This is the general form of the fully discrete, monolithic multiphysics system where the coupling predictor is unspecified. In the general setting where each coupling predictor depends on the state of all systems, the Jacobian of the coupling predictor is block dense with potentially sparse blocks

$$\frac{\partial \tilde{\mathbf{c}}}{\partial \mathbf{u}} = \begin{bmatrix} \frac{\partial \tilde{\mathbf{c}}^1}{\partial \mathbf{u}^1} & \cdots & \frac{\partial \tilde{\mathbf{c}}^1}{\partial \mathbf{u}^m} \\ \vdots & \ddots & \vdots \\ \frac{\partial \tilde{\mathbf{c}}^m}{\partial \mathbf{u}^1} & \cdots & \frac{\partial \tilde{\mathbf{c}}^m}{\partial \mathbf{u}^m} \end{bmatrix}. \quad (16)$$

This implies the Jacobian of the implicit velocity

$$D_{\mathbf{u}}\mathbf{g} = \frac{\partial \mathbf{r}}{\partial \mathbf{u}} + \frac{\partial \mathbf{r}}{\partial \tilde{\mathbf{c}}} \frac{\partial \tilde{\mathbf{c}}}{\partial \mathbf{u}} \quad (17)$$

is also block dense, which highlights the fact that there is coupling across all systems and a monolithic solver is required for the implicit step. The next section will introduce four coupling predictors that reduce the monolithic nature of the multiphysics IMEX-RK discretization to a partitioned scheme.

### 3.2.2. Four coupling predictors and reduction to partitioned schemes

To arrive at a scheme that can be solved in a *partitioned* way, we introduce four predictors that break the monolithic nature of the multiphysics system. The proposed predictors will first be classified as leading to a *weak* or *strong* coupling depending on whether the diagonal of the coupling predictor Jacobian is nonzero, i.e.,

$$\frac{\partial \tilde{\mathbf{c}}^i}{\partial \mathbf{u}^i} = 0 \quad \text{weakly coupled}, \quad \frac{\partial \tilde{\mathbf{c}}^i}{\partial \mathbf{u}^i} \neq 0 \quad \text{strongly coupled} \quad (18)$$

for  $i = 1, \dots, m$ . In other words, for the weakly coupled predictor, the predicted interaction force  $\tilde{\mathbf{c}}^i$  is constant with respect to the subsystem state  $\mathbf{u}^i$ . The predictors will further be classified based on whether they lead to a Jacobi-type (diagonal) or Gauss-Seidel-type (triangular) coupling, i.e.,

$$\frac{\partial \tilde{\mathbf{c}}^i}{\partial \mathbf{u}^j} = 0 \quad i \neq j \quad \text{Jacobi-type}, \quad \frac{\partial \tilde{\mathbf{c}}^i}{\partial \mathbf{u}^j} = 0 \quad i < j \quad \text{Gauss-Seidel-type}. \quad (19)$$

The remainder of this section is devoted to detailing the four predictors, the partitioned IMEX schemes that arise, and the advantages and disadvantages of each.

#### Weakly coupled Jacobi-type predictor

The first and simplest predictor is the weakly coupled Jacobi-type predictor that does not consider the instantaneous solution for *any* of the systems and only considers time history data, i.e.,

$$\tilde{\mathbf{c}}(\mathbf{u}, \bar{\mathbf{u}}, t) = \mathbf{c}(\bar{\mathbf{u}}, t). \quad (20)$$

At the fully discrete level, this predictor takes the form

$$\tilde{\mathbf{c}}(\mathbf{u}_{n,j}, \mathbf{u}_{n-1}, t) = \mathbf{c}(\mathbf{u}_{n-1}, t), \quad (21)$$

where  $\mathbf{u}_n$  is the multiphysics state vector at time step  $n$  (the previous time step) and  $\mathbf{u}_{n,j}$  is the approximation to  $\mathbf{u}_{n+1}$  at stage  $j$  of time step  $n$ , as defined in (11). In the context of the IMEX-RK discretization in (11), this predictor corresponds to lagging the coupling term to the previous time step throughout all stages of the time step. With this predictor, the IMEX-RK discretization of the multiphysics system in (11) leads to Algorithm 2.

---

**Algorithm 2** Implicit-Explicit Runge-Kutta partitioned multiphysics scheme: weak Jacobi predictor
 

---

- 1: **for** stages  $j = 1, \dots, s$  **do**
  - 2:   **for** physical systems  $i = 1, \dots, m$  **do**
  - 3:     Define stage solution according to (11a):  $\mathbf{u}_{n,j}^i = \mathbf{u}_{n-1}^i + \sum_{p=1}^{j-1} \hat{a}_{jp} \hat{\mathbf{k}}_{n,p}^i + \sum_{p=1}^j a_{jp} \mathbf{k}_{n,p}^i$
  - 4:     Implicit solve (11b) for  $\mathbf{k}_{n,j}^i$ :  $\mathbf{M}^i \mathbf{k}_{n,j}^i = \Delta t_n \mathbf{g}^i(\mathbf{u}_{n,j}^i, \mathbf{c}^i(\mathbf{u}_{n-1}^1, \dots, \mathbf{u}_{n-1}^m, t_{n,j}), t_{n,j})$
  - 5:     Explicit solve (11c) for  $\hat{\mathbf{k}}_{n,j}^i$ :  $\mathbf{M}^i \hat{\mathbf{k}}_{n,j}^i = \Delta t_n \mathbf{f}^i(\mathbf{u}_{n,j}^i, \mathbf{c}^i(\mathbf{u}_{n-1}^1, \dots, \mathbf{u}_{n-1}^m, t_{n,j}), t_{n,j})$
  - 6:   **end for**
  - 7: **end for**
  - 8: Set  $\mathbf{u}_n = \mathbf{u}_{n-1} + \sum_{p=1}^s \hat{b}_p \hat{\mathbf{k}}_{n,p} + \sum_{p=1}^s b_p \mathbf{k}_{n,p}$
- 

The IMEX-RK discretization with this coupling predictor is interpreted as, at each stage, an implicit solve that simultaneously accounts for all physics systems with the coupling term lagged one time step and corrected by an explicit step that accounts for the error introduced due to this lagged coupling term. Furthermore, this choice of predictor leads to a Jacobi-type decoupling of the various systems during the implicit solve at a given stage, thus allowing the monolithic system to be solved in a partitioned manner. This can easily be seen from the fact that the implicit Jacobian  $D_{\mathbf{u}}\mathbf{g}$  is block diagonal

$$D_{\mathbf{u}}\mathbf{g} = \frac{\partial \mathbf{r}}{\partial \mathbf{u}} \quad (22)$$

since the Jacobian of the coupling predictor is zero and  $\frac{\partial \mathbf{r}}{\partial \mathbf{u}}$  is block diagonal from (9).

There are a number of advantages surrounding the weak Jacobi-type coupling predictor, mostly pertaining to simplicity and efficiency. First, the implicit Jacobian (13b) does not require the Jacobian of the coupling term, which can be cumbersome to implement, particularly when used to patch together existing software to form a multiphysics tool. Additionally, this simple predictor allows maximum re-use of single-physics software since only the coupling term must be communicated between codes to implement the multiphysics partitioned scheme. Once communication of the coupling term is complete at the beginning of a time step, the Jacobi-type coupling implies that, within a given time step, all single-physics systems are independent and can be performed in parallel. Finally, since the partitioned discretization is a special case of the IMEX-RK discretization in (11), it is guaranteed to preserve the design order of the discretization; see Section 3.2.4 for a detailed discussion. The primary disadvantage of this simple and efficient predictor is reduced stability properties, which will be discussed further in Section 3.2.4.

#### *Strongly coupled Jacobi-type predictor*

A predictor that maintains a Jacobi-type coupling, i.e., block diagonal implicit Jacobian, while incorporating additional instantaneous information is defined as

$$\tilde{\mathbf{c}}^i(\mathbf{u}, \bar{\mathbf{u}}, t) = \mathbf{c}(\bar{\mathbf{u}}^1, \dots, \bar{\mathbf{u}}^{i-1}, \mathbf{u}^i, \bar{\mathbf{u}}^{i+1}, \dots, \bar{\mathbf{u}}^m, t). \quad (23)$$

for  $i = 1, \dots, m$ . At the fully discrete level, this predictor takes the form

$$\tilde{\mathbf{c}}^i(\mathbf{u}_{n,j}, \mathbf{u}_{n-1}, t) = \mathbf{c}(\mathbf{u}_{n-1}^1, \dots, \mathbf{u}_{n-1}^{i-1}, \mathbf{u}_{n,j}^i, \mathbf{u}_{n-1}^{i+1}, \dots, \mathbf{u}_{n-1}^m, t). \quad (24)$$

This leads to a strong coupling where  $\frac{\partial \tilde{\mathbf{c}}^i}{\partial \mathbf{u}^i} \neq 0$ . In the context of the IMEX-RK discretization in (11), the strong Jacobi predictor corresponds to using the instantaneous state for the  $i$ th system in the  $i$ th coupling term and lagging the remaining states to the previous time step. With this predictor, the IMEX-RK discretization of the multiphysics system leads to Algorithm 3.

---

**Algorithm 3** Implicit-Explicit Runge-Kutta partitioned multiphysics scheme: strong Jacobi predictor
 

---

- 1: **for** stages  $j = 1, \dots, s$  **do**
  - 2:   **for** physical systems  $i = 1, \dots, m$  **do**
  - 3:     Define stage solution according to (11a):  $\mathbf{u}_{n,j}^i = \mathbf{u}_{n-1}^i + \sum_{p=1}^{j-1} \hat{a}_{jp} \hat{\mathbf{k}}_{n,p}^i + \sum_{p=1}^j a_{jp} \mathbf{k}_{n,p}^i$
  - 4:     Implicit solve (11b) for  $\mathbf{k}_{n,j}^i$ :  $\mathbf{M}^i \mathbf{k}_{n,j}^i = \Delta t_n \mathbf{g}^i(\mathbf{u}_{n,j}^i, \mathbf{c}^i(\mathbf{u}_{n-1}^1, \dots, \mathbf{u}_{n-1}^{i-1}, \mathbf{u}_{n,j}^i, \mathbf{u}_{n-1}^{i+1}, \dots, \mathbf{u}_{n-1}^m, t_{n,j}), t_{n,j})$
  - 5:     Explicit solve (11c) for  $\hat{\mathbf{k}}_{n,j}^i$ :  $\mathbf{M}^i \hat{\mathbf{k}}_{n,j}^i = \Delta t_n \mathbf{f}^i(\mathbf{u}_{n,j}^i, \mathbf{c}^i(\mathbf{u}_{n-1}^1, \dots, \mathbf{u}_{n-1}^{i-1}, \mathbf{u}_{n,j}^i, \mathbf{u}_{n-1}^{i+1}, \dots, \mathbf{u}_{n-1}^m, t_{n,j}), t_{n,j})$
  - 6:   **end for**
  - 7: **end for**
  - 8: Set  $\mathbf{u}_n = \mathbf{u}_{n-1} + \sum_{p=1}^s \hat{b}_p \hat{\mathbf{k}}_{n,p} + \sum_{p=1}^s b_p \mathbf{k}_{n,p}$
- 

The interpretation of the IMEX-RK discretization with the strong Jacobi predictor is similar to that of the weak Jacobi predictor with the exception that the coupling term is not entirely lagged to the previous time step. The Jacobian of the coupling predictor in (23) is block diagonal

$$\frac{\partial \tilde{\mathbf{c}}}{\partial \mathbf{u}} = \begin{bmatrix} \frac{\partial \mathbf{c}^1}{\partial \mathbf{u}^1} & & & \\ & \ddots & & \\ & & \frac{\partial \mathbf{c}^m}{\partial \mathbf{u}^m} & \\ & & & \ddots \end{bmatrix}, \quad (25)$$

which leads to a block diagonal implicit Jacobian

$$D_{\mathbf{u}} \mathbf{g} = \begin{bmatrix} \frac{\partial \mathbf{r}^1}{\partial \mathbf{u}^1} + \frac{\partial \mathbf{r}^1}{\partial \mathbf{c}^1} \frac{\partial \mathbf{c}^1}{\partial \mathbf{u}^1} & & & \\ & \ddots & & \\ & & \frac{\partial \mathbf{r}^m}{\partial \mathbf{u}^m} + \frac{\partial \mathbf{r}^m}{\partial \mathbf{c}^m} \frac{\partial \mathbf{c}^m}{\partial \mathbf{u}^m} & \\ & & & \ddots \end{bmatrix}. \quad (26)$$

The strong Jacobi predictor shares some of the advantages as the weak Jacobi predictor such as a block diagonal implicit Jacobian that allows all systems to be solved simultaneously and the ability to re-use single physics software since only the coupling term must be communicated between codes. However, the  $i$ th system now requires the Jacobian of its own coupling term with respect to its own state, a term that may not be readily available or have an obvious data structure. The strong Jacobi predictor is guaranteed to preserve the design order of the IMEX-RK discretization and has better stability properties than the weak Jacobi predictor; see Section 3.2.4 for a detailed discussion.

#### *Weakly coupled Gauss-Seidel-type predictor*

The Gauss-Seidel-type (triangular) predictors for the multiphysics system assume the individual systems are *ordered* in a physically relevant manner. The preferred ordering is problem-dependent and a number of examples are provided in Sections 4-7. The weakly coupled Gauss-Seidel-type predictor for the  $i$ th system is defined as

$$\tilde{\mathbf{c}}^i(\mathbf{u}, \bar{\mathbf{u}}) = \mathbf{c}(\mathbf{u}^1, \dots, \mathbf{u}^{i-1}, \bar{\mathbf{u}}^i, \dots, \bar{\mathbf{u}}^m) \quad (27)$$

for  $i = 1, \dots, m$ . At the fully discrete level, this predictor takes the form

$$\tilde{\mathbf{c}}^i(\mathbf{u}_{n,j}, \mathbf{u}_{n-1}, t) = \mathbf{c}(\mathbf{u}_{n,j}^1, \dots, \mathbf{u}_{n,j}^{i-1}, \mathbf{u}_{n-1}^i, \dots, \mathbf{u}_{n-1}^m). \quad (28)$$

In the context of the IMEX-RK discretization in (11), the  $i$ th predictor lags the state of systems  $i, \dots, m$  to the previous time step in the evaluation of the coupling term throughout all stages of the time step.

The IMEX-RK discretization of the multiphysics system in (11) with this form of the predictor leads to Algorithm 4.

---

**Algorithm 4** Implicit-Explicit Runge-Kutta partitioned multiphysics scheme: weak Gauss-Seidel predictor

---

- 1: **for** stages  $j = 1, \dots, s$  **do**
  - 2:     **for** physical systems  $i = 1, \dots, m$  **do**
  - 3:         Define stage solution according to (11a):  $\mathbf{u}_{n,j}^i = \mathbf{u}_{n-1}^i + \sum_{p=1}^{j-1} \hat{a}_{jp} \hat{\mathbf{k}}_{n,p}^i + \sum_{p=1}^j a_{jp} \mathbf{k}_{n,p}^i$
  - 4:         Implicit solve (11b) for  $\mathbf{k}_{n,j}^i$ :  $M^i \mathbf{k}_{n,j}^i = \Delta t_n \mathbf{g}^i(\mathbf{u}_{n,j}^i, \mathbf{c}^i(\mathbf{u}_{n,j}^1, \dots, \mathbf{u}_{n,j}^{i-1}, \mathbf{u}_{n-1}^i, \dots, \mathbf{u}_{n-1}^m, t_{n,j}), t_{n,j})$
  - 5:         Explicit solve (11c) for  $\hat{\mathbf{k}}_{n,j}^i$ :  $M^i \hat{\mathbf{k}}_{n,j}^i = \Delta t_n \mathbf{f}^i(\mathbf{u}_{n,j}^i, \mathbf{c}^i(\mathbf{u}_{n,j}^1, \dots, \mathbf{u}_{n,j}^{i-1}, \mathbf{u}_{n-1}^i, \dots, \mathbf{u}_{n-1}^m, t_{n,j}), t_{n,j})$
  - 6:     **end for**
  - 7: **end for**
  - 8: Set  $\mathbf{u}_n = \mathbf{u}_{n-1} + \sum_{p=1}^s \hat{b}_p \hat{\mathbf{k}}_{n,p} + \sum_{p=1}^s b_p \mathbf{k}_{n,p}$
- 

In this case, the Jacobian of the coupling predictor is block strictly lower triangular

$$\frac{\partial \tilde{\mathbf{c}}}{\partial \mathbf{u}} = \begin{bmatrix} 0 & & & & \\ \frac{\partial \mathbf{c}^2}{\partial \mathbf{u}^1} & 0 & & & \\ \vdots & \ddots & \ddots & & \\ \frac{\partial \mathbf{c}^m}{\partial \mathbf{u}^1} & \cdots & \frac{\partial \mathbf{c}^m}{\partial \mathbf{u}^{m-1}} & 0 & \end{bmatrix}, \quad (29)$$

which implies the Jacobian of the monolithic implicit system is block lower triangular

$$D_{\mathbf{u}^j} \mathbf{g}^i = \begin{cases} \frac{\partial \mathbf{r}^i}{\partial \mathbf{u}^i} & i = j \\ \frac{\partial \mathbf{r}^i}{\partial \mathbf{c}^i} \frac{\partial \mathbf{c}^i}{\partial \mathbf{u}^j} & i > j \\ \mathbf{0} & i < j. \end{cases} \quad (30)$$

This block lower triangular nature of the monolithic implicit system implies that the individual systems can be solved sequentially beginning with system 1 and yields a partitioned scheme.

The implicit Jacobian of the monolithic implicit system of the weak Gauss-Seidel predictor (30) involves the entire lower triangular portion of the coupling predictor; however, it is *not required* for the implementation. From inspection of Algorithm 4, the implicit phase at stage  $j$  for the  $i$ th physical system requires the solution of a nonlinear system of equations in the variable  $\mathbf{u}_{n,j}^i$ , with  $\mathbf{u}_{n,j}^1, \dots, \mathbf{u}_{n,j}^{i-1}$  available from the implicit solve corresponding to previous physical systems at the current stage. Therefore, only the *diagonal terms*  $\frac{D\mathbf{g}^i}{D\mathbf{u}^i} = \frac{\partial \mathbf{r}^i}{\partial \mathbf{u}^i}$  of the monolithic implicit Jacobian are required, which shows that the Jacobians of the coupling terms are not required for the weak Gauss-Seidel predictor. Compared with Jacobi-type predictors, the Gauss-Seidel-type predictor also requires the systems be solved serially within each Runge-Kutta stage and therefore forfeits the opportunity to parallelize across systems. This predictor is guaranteed to preserve the design order of the IMEX-RK discretization and possesses similar stability properties to the weak Jacobi predictor; see Section 3.2.4. In Section 6 we show some desirable properties of the weak Gauss-Seidel predictor that arise in practice.

*Strongly coupled Gauss-Seidel-type predictor*

A strong Gauss-Seidel-type coupling is obtained if the  $i$ th coupling predictor considers the instantaneous solution for systems  $1, \dots, i$  and the time history for the remaining systems, i.e.,

$$\tilde{\mathbf{c}}^i(\mathbf{u}, \bar{\mathbf{u}}, t) = \mathbf{c}(\mathbf{u}^1, \dots, \mathbf{u}^i, \bar{\mathbf{u}}^{i+1}, \dots, \bar{\mathbf{u}}^m, t) \quad (31)$$

for  $i = 1, \dots, m$ . At the fully discrete level, this predictor takes the form

$$\tilde{\mathbf{c}}^i(\mathbf{u}_{n,j}, \mathbf{u}_{n-1}, t) = \mathbf{c}(\mathbf{u}_{n,j}^1, \dots, \mathbf{u}_{n,j}^i, \mathbf{u}_{n-1}^{i+1}, \dots, \mathbf{u}_{n-1}^m). \quad (32)$$

In the context of the IMEX-RK discretization in (11), the  $i$ th predictor lags the state of systems  $i+1, \dots, m$  to the previous time step in the evaluation of the coupling term throughout all stages of the time step. The IMEX-RK discretization of the multiphysics system in (11) with the strong Gauss-Seidel predictor becomes Algorithm 5.

---

**Algorithm 5** Implicit-Explicit Runge-Kutta partitioned multiphysics scheme: strong Gauss-Seidel predictor

---

- 1: **for** stages  $j = 1, \dots, s$  **do**
  - 2:     **for** physical systems  $i = 1, \dots, m$  **do**
  - 3:         Define stage solution according to (11a):  $\mathbf{u}_{n,j}^i = \mathbf{u}_{n-1}^i + \sum_{p=1}^{j-1} \hat{a}_{jp} \hat{\mathbf{k}}_{n,p}^i + \sum_{p=1}^j a_{jp} \mathbf{k}_{n,p}^i$
  - 4:         Implicit solve (11b) for  $\mathbf{k}_{n,j}^i$ :  $\mathbf{M}^i \mathbf{k}_{n,j}^i = \Delta t_n \mathbf{g}^i(\mathbf{u}_{n,j}^i, \mathbf{c}^i(\mathbf{u}_{n,j}^1, \dots, \mathbf{u}_{n,j}^i, \mathbf{u}_{n-1}^{i+1}, \dots, \mathbf{u}_{n-1}^m, t_{n,j}), t_{n,j})$
  - 5:         Explicit solve (11c) for  $\hat{\mathbf{k}}_{n,j}^i$ :  $\mathbf{M}^i \hat{\mathbf{k}}_{n,j}^i = \Delta t_n \mathbf{f}^i(\mathbf{u}_{n,j}^i, \mathbf{c}^i(\mathbf{u}_{n,j}^1, \dots, \mathbf{u}_{n,j}^i, \mathbf{u}_{n-1}^{i+1}, \dots, \mathbf{u}_{n-1}^m, t_{n,j}), t_{n,j})$
  - 6:     **end for**
  - 7: **end for**
  - 8: Set  $\mathbf{u}_n = \mathbf{u}_{n-1} + \sum_{p=1}^s \hat{b}_p \hat{\mathbf{k}}_{n,p} + \sum_{p=1}^s b_p \mathbf{k}_{n,p}$
- 

The Jacobian of the coupling predictor is block lower triangular

$$\frac{\partial \tilde{\mathbf{c}}}{\partial \mathbf{u}} = \begin{bmatrix} \frac{\partial \mathbf{c}^1}{\partial \mathbf{u}^1} & & & \\ \vdots & \ddots & & \\ \frac{\partial \mathbf{c}^m}{\partial \mathbf{u}^1} & \dots & \frac{\partial \mathbf{c}^m}{\partial \mathbf{u}^m} & \\ \vdots & & & \ddots \end{bmatrix}, \quad (33)$$

which implies that the Jacobian of the monolithic implicit system is also block lower triangular

$$D_{\mathbf{u}^i} \mathbf{g}^i = \begin{cases} \frac{\partial \mathbf{r}^i}{\partial \mathbf{u}^i} + \frac{\partial \mathbf{r}^i}{\partial \mathbf{c}^i} \frac{\partial \mathbf{c}^i}{\partial \mathbf{u}^i} & i = j \\ \frac{\partial \mathbf{r}^i}{\partial \mathbf{c}^i} \frac{\partial \mathbf{c}^i}{\partial \mathbf{u}^j} & i > j \\ \mathbf{0} & i < j. \end{cases} \quad (34)$$

Similar to the weak Gauss-Seidel-type predictor, this block lower triangular nature of the monolithic implicit system implies that the individual systems can be solved sequentially beginning with system 1 and yields a partitioned scheme.

The strong Gauss-Seidel predictor uses as much current information as possible while guaranteeing a partitioned scheme and the design accuracy of the IMEX-RK discretization is not reduced. Similar to the weak Gauss-Seidel predictor, only the diagonal terms  $\frac{D \mathbf{g}^i}{D \mathbf{u}^i} = \frac{\partial \mathbf{r}^i}{\partial \mathbf{u}^i} + \frac{\partial \mathbf{r}^i}{\partial \mathbf{c}^i} \frac{\partial \mathbf{c}^i}{\partial \mathbf{u}^i}$  of the monolithic implicit Jacobian are required. The implementation effort is only slightly higher than the weak Gauss-Seidel predictor

given that the diagonal of the coupling Jacobian is required. It will be shown in Section 3.2.4 that the inclusion of these diagonal terms leads to enhanced stability properties.

In general, strong coupling predictors include contributions to the block diagonal from the coupling term, which improves the stability of the resulting partitioned scheme, but requires more implementation effort than the weak coupling counterparts. Gauss-Seidel-type predictors lead to partitioned algorithms where the individual physical subsystems must be solved sequentially, which reduces their efficiency compared to Jacobi-type predictors.

### 3.2.3. A special case of the coupling structure

The aforementioned implicit-explicit decomposition with the coupling predictor (Section 3.2.2) is the most general form of the splitting; however, it does not take advantage of any special structure in the multiphysics problems since we must predict all  $m$  interactions to decouple the multiphysics system. For many multiphysics problems, such as two-field coupling problems, three-field fluid-structure-interaction, and magnetohydrodynamics, the following coupling structure exists

$$\begin{aligned} \mathbf{c}^1 &= \mathbf{c}^1(\mathbf{u}^1, \dots, \mathbf{u}^m, t) \\ \mathbf{c}^i &= \mathbf{c}^i(\mathbf{u}^1, \dots, \mathbf{u}^i, t) \quad i = 2, \dots, m. \end{aligned} \quad (35)$$

The strong Gauss-Seidel coupling predictor applied to a coupling term with the above structure yields

$$\begin{aligned} \tilde{\mathbf{c}}^1(\mathbf{u}, \bar{\mathbf{u}}, t) &= \mathbf{c}(\mathbf{u}^1, \bar{\mathbf{u}}^2, \dots, \bar{\mathbf{u}}^m, t) \\ \tilde{\mathbf{c}}^i(\mathbf{u}, \bar{\mathbf{u}}, t) &= \mathbf{c}(\mathbf{u}^1, \dots, \mathbf{u}^i, t) \quad i = 2, \dots, m \end{aligned} \quad (36)$$

and therefore the coupling predictors for systems  $2, \dots, m$  are exact, i.e., identical to the true coupling term. This implies only a single predictor  $\tilde{\mathbf{c}}^1$  is needed to decouple the multiphysics system and arrive at a partitioned scheme. In this case, the explicit and implicit terms of the IMEX-RK scheme reduce to

$$\mathbf{f}(\mathbf{u}, \tilde{\mathbf{c}}, t) = \begin{bmatrix} \mathbf{r}^1(\mathbf{u}^1, \mathbf{c}^1, t) - \mathbf{r}^1(\mathbf{u}^1, \tilde{\mathbf{c}}^1, t) \\ \mathbf{0} \\ \vdots \\ \mathbf{0} \end{bmatrix}, \quad \mathbf{g}(\mathbf{u}, \tilde{\mathbf{c}}, t) = \begin{bmatrix} \mathbf{r}^1(\mathbf{u}^1, \tilde{\mathbf{c}}^1, t) \\ \mathbf{r}^2(\mathbf{u}^2, \mathbf{c}^2, t) \\ \vdots \\ \mathbf{r}^m(\mathbf{u}^m, \mathbf{c}^m, t) \end{bmatrix} \quad (37)$$

In Section 4-7, a series of applications that possess this special coupling structure are presented.

### 3.2.4. Accuracy and stability analysis

The accuracy of implicit-explicit Runge-Kutta schemes is analyzed in detail in [15, 20, 19, 21], where order conditions are derived from the Taylor expansion of the exact and numerical solution. Generally,  $p$ th order IMEX schemes have local truncation error of  $\mathcal{O}(\Delta t^{p+1})$  during one time step  $[t_{n-1}, t_{n-1} + \Delta t]$  and therefore global temporal error  $\mathcal{O}(\Delta t^p)$ . Great care was taken in Section 3.2.2 to introduce the proposed predictor-based, partitioned multiphysics scheme as an implicit-explicit Runge-Kutta discretization to emphasize that the design order of the IMEX-RK scheme applied to the monolithic multiphysics system is inherited. This is only possible because the chosen predictors have an interpretation at the *semi-discrete* level; predictors that combine stage information in a heuristic way [16, 17] may in general suffer from order reduction, which will be demonstrated in Section 4. Therefore, incorporating any of the four proposed predictors into a  $p$ th order IMEX-RK schemes leads to the same  $\mathcal{O}(\Delta t^{p+1})$  local truncation error and the same  $\mathcal{O}(\Delta t^p)$  global temporal error.

To study the linear stability of the partitioned IMEX-RK schemes, we consider the coupled, stable, linear model problem

$$\begin{aligned} \partial_t u^1 &= \lambda_1(u^1 + u^2) \\ \partial_t u^2 &= \lambda_2(u^1 + u^2), \end{aligned} \quad (38)$$

where  $\Re(\lambda_1) < 0$  and  $\Re(\lambda_2) < 0$ , that will exhibit the crux of the linear stability issues for first-order systems such as advection-diffusion-reaction and particle-laden flow. However, it does not model complex bi-directional coupling, e.g., characteristic of many problems in magnetohydrodynamics; see Appendix A for analysis of a general linear system of ODEs. This system can be written compactly as

$$\mathbf{M}\dot{\mathbf{u}} = \mathbf{r}(\mathbf{u}, \mathbf{c}(\mathbf{u})), \quad (39)$$

where

$$\mathbf{M} = \begin{bmatrix} 1 & \\ & 1 \end{bmatrix}, \quad \mathbf{u} = \begin{bmatrix} u^1 \\ u^2 \end{bmatrix}, \quad \mathbf{c}(\mathbf{u}) = \begin{bmatrix} c^1(u^1, u^2) \\ c^2(u^1, u^2) \end{bmatrix}, \quad \mathbf{r}(\mathbf{u}, \mathbf{c}) = \begin{bmatrix} (1-\alpha)\lambda_1 u^1 + \lambda_1 c^1 \\ (1-\alpha)\lambda_2 u^2 + \lambda_2 c^2 \end{bmatrix} \quad (40)$$

The coupling terms are chosen as  $c^1(u^1, u^2) = \alpha u^1 + u^2$ ,  $c^2(u^1, u^2) = u^1 + \alpha u^2$ , and  $\alpha \in \mathbb{R}$  is a coupling parameter that varies the extent to which an evolution equation depends on its own state directly through the velocity term or the coupling term, an important distinction when comparing the weak and strong predictors. For values of  $\alpha$  near unity, the  $i$ th evolution equation depends on  $u^i$  mostly through the coupling term, whereas  $\alpha$  near zero implies the dependence is directly through the uncoupled velocity term. The four predictor-based IMEX schemes introduced in 3.2.2 are applied to this model problem. The predictor and associated implicit-explicit partition for each are provided in the Table 2.

	$\tilde{\mathbf{c}}$	$\mathbf{g}$	$\mathbf{f}$
Weak Jacobi	$\begin{bmatrix} \alpha \bar{u}^1 + \bar{u}^2 \\ \alpha \bar{u}^2 + \bar{u}^1 \end{bmatrix}$	$\begin{bmatrix} \lambda_1((1-\alpha)u^1 + \alpha \bar{u}^1 + \bar{u}^2) \\ \lambda_2((1-\alpha)u^2 + \alpha \bar{u}^2 + \bar{u}^1) \end{bmatrix}$	$\begin{bmatrix} \lambda_1 \alpha (u^1 - \bar{u}^1) + \lambda_1 (u^2 - \bar{u}^2) \\ \lambda_2 \alpha (u^2 - \bar{u}^2) + \lambda_2 (u^1 - \bar{u}^1) \end{bmatrix}$
Strong Jacobi	$\begin{bmatrix} \alpha u^1 + \bar{u}^2 \\ \alpha u^2 + \bar{u}^1 \end{bmatrix}$	$\begin{bmatrix} \lambda_1 (u^1 + \bar{u}^2) \\ \lambda_2 (\bar{u}^1 + u^2) \end{bmatrix}$	$\begin{bmatrix} \lambda_1 (u^2 - \bar{u}^2) \\ \lambda_2 (u^1 - \bar{u}^1) \end{bmatrix}$
Weak Gauss-Seidel	$\begin{bmatrix} \alpha \bar{u}^1 + \bar{u}^2 \\ \alpha \bar{u}^2 + u^1 \end{bmatrix}$	$\begin{bmatrix} \lambda_1((1-\alpha)u^1 + \alpha \bar{u}^1 + \bar{u}^2) \\ \lambda_2((1-\alpha)u^2 + \alpha \bar{u}^2 + u^1) \end{bmatrix}$	$\begin{bmatrix} \lambda_1 \alpha (u^1 - \bar{u}^1) + \lambda_1 (u^2 - \bar{u}^2) \\ \lambda_2 \alpha (u^2 - \bar{u}^2) \end{bmatrix}$
Strong Gauss-Seidel	$\begin{bmatrix} \alpha u^1 + \bar{u}^2 \\ \alpha u^2 + u^1 \end{bmatrix}$	$\begin{bmatrix} \lambda_1 (u^1 + \bar{u}^2) \\ \lambda_2 (u^1 + u^2) \end{bmatrix}$	$\begin{bmatrix} \lambda_1 (u^2 - \bar{u}^2) \\ 0 \end{bmatrix}$

Table 2: The partition of Eq. (38) based on weak/strong predictors and Jacobi/Gauss-Seidel strategies

In this section, we consider the 1st-order forward-backward Euler IMEX scheme [15]; the linear stability analysis of the other IMEX schemes considered in this work is provided in Appendix A.

Explicit Runge-Kutta coefficients

$$\begin{array}{c|ccc} 0 & 0 & 0 \\ 1 & 1 & 0 \\ 0 & 1 & 0 \end{array}$$

Implicit Runge-Kutta coefficients

$$\begin{array}{c|ccc} 0 & 0 & 0 \\ 1 & 0 & 1 \\ 0 & 0 & 1 \end{array}$$

The forward-backward Euler IMEX scheme applied to the system in (39)-(40) yields the one-step update

equation

$$\mathbf{u}_n = \mathbf{u}_{n-1} + \Delta t(\mathbf{f}(\mathbf{u}_{n-1}) + \mathbf{g}(\mathbf{u}_n)) \quad (41)$$

that can be re-written as

$$\mathbf{u}_n = \mathbf{C}(\Delta t, \lambda_1, \lambda_2, \alpha)\mathbf{u}_{n-1}. \quad (42)$$

once the partitions in Table 2 are introduced. An update equation of this form is stable if the spectral radius of the matrix satisfies

$$\rho(\mathbf{C}) \leq 1, \quad (43)$$

and the multiplicity of any eigenvalues of magnitude 1 is equal to the dimension of its eigenspace.

The spectral radius and the region of unconditional stability for the 1st-order IMEX scheme based on the partitions in Table 2 are provided in Table 3. Both strong predictors lead to unconditional stability, regardless of the value of  $\alpha$ , while the stable regions for the weak predictors depend on the coupling strength. The weak Gauss-Seidel predictor has a larger  $\alpha$ -range of unconditional stability than the weak Jacobi predictor which is only stable for  $\alpha \leq 0$ . The high-order IMEX-RK schemes considered in this work are analyzed in Appendix A and the strong Gauss-Seidel predictors are shown to be unconditionally stable, regardless of  $\alpha$ , while the strong Jacobi predictor is not.

	Spectral radius	Unconditional stability range
Weak Jacobi	$\max \left\{ 1, \left  \frac{(1 + \alpha\Delta t\lambda_1)(1 + \alpha\Delta t\lambda_2) - \Delta t^2\lambda_1\lambda_2}{(1 - (1 - \alpha)\Delta t\lambda_2)(1 - (1 - \alpha)\Delta t\lambda_1)} \right  \right\}$	$\alpha \leq 0$
Strong Jacobi	$\max \left\{ 1, \left  \frac{1 - \Delta t^2\lambda_1\lambda_2}{(1 - \Delta t\lambda_1)(1 - \Delta t\lambda_2)} \right  \right\}$	$\forall \alpha$
Weak Gauss-Seidel	$\max \left\{ 1, \left  \frac{(1 + \alpha\Delta t\lambda_1)(1 + \alpha\Delta t\lambda_2)}{(1 - (1 - \alpha)\Delta t\lambda_1)(1 - (1 - \alpha)\Delta t\lambda_2)} \right  \right\}$	$\alpha \leq 0.5$
Strong Gauss-Seidel	$\max \left\{ 1, \left  \frac{1}{(1 - \Delta t\lambda_1)(1 - \Delta t\lambda_2)} \right  \right\}$	$\forall \alpha$

Table 3: The iterative matrix spectrum radius and unconditional stability range of the 1st-order IMEX based on weak/strong predictors and Jacobi/Gauss-Seidel strategies

We close this section by demonstrating that the unconditional linear stability result requires analyzing the chosen numerical scheme applied to the entire coupled system, rather than using the exact solution of one subsystem to reduce to the problem to a single system with added-mass [13]. The exact solution of the model problem Eq. (38) with the initial condition

$$u^2(0) = \frac{\lambda_2}{\lambda_1} u^1(0) \quad (44)$$

takes the form

$$u^2(t) = \frac{\lambda_2}{\lambda_1} u^1(t). \quad (45)$$

From Table 2, the partitioned scheme resulting from the 1st-order, 2-stage IMEX-RK scheme with strong Gauss-Seidel predictor leads to the one-step update equation

$$u_n^1 = u_{n-1}^1 + \Delta t \lambda_1 (u_n^1 + u_{n-1}^2) \quad (46a)$$

$$u_n^2 = u_{n-1}^2 + \Delta t \lambda_2 (u_n^1 + u_n^2), \quad (46b)$$

which was determined to be unconditionally stable; see Table 3. However, this scheme can be analyzed solely in terms of the equation for  $u_n^1$  by substituting the exact solution for  $u^2$  into Eq. (46a)

$$u_n^1 = u_{n-1}^1 + \Delta t \lambda_1 u_n^1 + \Delta t \lambda_2 u_{n-1}^1. \quad (47)$$

In this case, the scheme is only conditionally stable

$$\left| \frac{1 + \Delta t \lambda_2}{1 - \Delta t \lambda_1} \right| \leq 1, \quad (48)$$

which illustrates how the artificial decoupling brought into the analysis through the exact solution can degenerate stability.

#### 4. Application to a coupled system of ordinary differential equations

In this section, we study the proposed high-order partitioned solvers and predictors on a  $3 \times 3$  system of linear Ordinary Differential Equations (ODEs)

$$\dot{\mathbf{u}} = \mathcal{A}\mathbf{u}, \quad \mathcal{A} = \begin{bmatrix} 1 & 1 & 1 \\ 1 & 1 & 0 \\ 1 & 1 & 1 \end{bmatrix}, \quad \mathbf{u} = \begin{bmatrix} u^1 \\ u^2 \\ u^3 \end{bmatrix} \quad (49)$$

with initial condition  $\mathbf{u}(0) = (1, 0, 2)^T$  and consider the time domain  $t \in (0, 2]$ . The exact solution at any time  $t$  is given in terms of the initial condition and the eigenvalue decomposition of the coefficient matrix,  $\mathcal{A}\mathcal{P} = \mathcal{P}\Sigma$ , as

$$\mathbf{u}(t) = \mathcal{P}e^{t\Sigma}\mathcal{P}^{-1}\mathbf{u}(0). \quad (50)$$

To conform to the multiphysics formulation in (3) the ODE system is treated as a coupled system with three subsystems. The mass matrix is identity, the velocity term is taken as

$$\mathbf{r} = (\mathbf{u}^1 + \mathbf{c}^1, \mathbf{u}^2 + \mathbf{c}^2, \mathbf{u}^3 + \mathbf{c}^3)^T, \quad (51)$$

and the coupling terms are defined as

$$\mathbf{c}^1 = \mathbf{u}^2 + \mathbf{u}^3, \quad \mathbf{c}^2 = \mathbf{u}^1, \quad \mathbf{c}^3 = \mathbf{u}^1 + \mathbf{u}^2. \quad (52)$$

This decomposition of the velocity is non-unique. In fact, many other choices exist that will lead to different schemes; however, the above choice is the most sensible since it mimics the multiphysics applications we are targeting and possesses special structure. In particular,  $\mathbf{c}^i$  does not depend on  $\mathbf{u}^i$  and therefore the strong predictors and weak predictors are equivalent. Additionally, the coupling term possesses the same structure as Eq. (35), which implies only  $\tilde{\mathbf{c}}^1$  is required for the strong Gauss-Seidel predictor.

To validate the temporal convergence of the high-order partitioned scheme, we apply the 2nd-order 2-stage trapezoidal rule, 3rd-order 4-stage ARK3(2)4L[2]SA, and 4th-order 6 stage ARK4(3)6L[2]SA [19] to the ODE system in (49). These schemes will be abbreviated by IMEX2, IMEX3, and IMEX4, respectively.

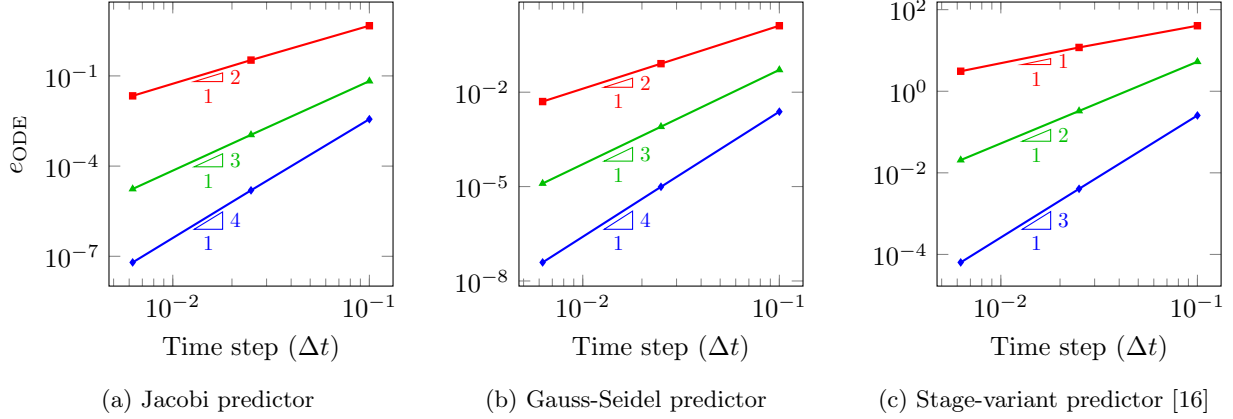


Figure 1: Convergence of the IMEX2 (—■—), IMEX3 (—▲—), and IMEX4 (—●—) schemes with various predictors as applied to the ODE system.

For a given IMEX-RK scheme, three different predictors are tested. The first two are the Jacobi and Gauss-Seidel predictors proposed in Section 3.2.2; recall there is no distinction between weak and strong predictors given the structure of the coupling term. We also consider the predictor proposed in [17, 16] for two-field fluid-structure interaction problems, which is a Gauss-Seidel-type predictor

$$\tilde{\mathbf{c}}_{n,j}^1 = \sum_{k=1}^{j-1} \frac{\hat{a}_{jk} - a_{jk}}{\hat{a}_{jj}} \mathbf{c}_{n,k}^1 \quad (53)$$

for stages  $j = 2, \dots, s$ , where  $\mathbf{c}_{n,k}^1 = \mathbf{u}_{n,k}^2 + \mathbf{u}_{n,k}^3$ , and  $\hat{a}_{ki}$  and  $a_{ki}$  are the Butcher coefficients of the ERK and ESDIRK schemes, respectively, in Table 1. Unlike the predictors proposed in this work, this predictor is stage-dependent and does not have an interpretation at the ODE level. Therefore it is not guaranteed to preserve the design order of the IMEX scheme, even though it does so empirically in [16, 17].

The accuracy is quantified via the  $L_\infty$ -norm of the error in the numerical solution at time  $t = 2.0$

$$e_{\text{ODE}} = \max_{1 \leq i \leq 3} |\mathbf{u}_N^i - \mathbf{u}^i(2)|, \quad (54)$$

where  $\mathbf{u}^i(2)$  is the exact solution at  $t = 2.0$  and  $\mathbf{u}_N^i$  the numerical solution at the final time step for the  $i$ th subsystem. The error  $e_{\text{ODE}}$  as a function of the time step size for the second, third, and fourth order IMEX-RK methods are shown in Figure 1. Note that in Figure 1a and Figure 1b, the schemes exhibit convergence at the design rate of the IMEX scheme and the error with the Gauss-Seidel predictor is several times smaller than that of the Jacobi predictor due to different error constants. However, the stage-variant predictor in Figure 1c results in a scheme with an order of accuracy one less than the design order.

## 5. Application to time-dependent advection-diffusion-reaction equations

In this section, we consider time-dependent coupled advection-diffusion-reaction (ADR) systems that have applications in the modeling of chemical reactions [22], the description for superconductivity of liquids [23], and biological predator-prey models [24]. The governing equation for the  $i$ th species in a general ADR system with  $n$  components in  $d$ -dimensions is

$$\frac{\partial u^i}{\partial t} + (v^i \cdot \nabla) u^i - \nabla(D^i \cdot \nabla u^i) = f^i(u, x, t), \quad (x, t) \in v \times (0, 1], \quad 1 \leq i \leq n. \quad (55)$$

Here,  $u = [u^1 \ \cdots \ u^n]^T$  contains the  $n$  conserved quantities modeled by the ADR equations,  $\Omega \subset \mathbb{R}^d$  is the computational domain,  $D^i \in \mathbb{R}^{d \times d}$  is the diffusivity matrix and  $v^i(x) \in \mathbb{R}^d$  is the velocity field for the  $i$ th species. In this work, we consider the predator-prey model from [24], which involves  $n = 2$  coupled systems with

$$f^1(u, x, t) = u^1(-(u^1 - a^1)(u^1 - 1) - a^2 u^2) \quad f^2(u, x, t) = u^2(-a^3 - a^4 u^2 + a^2 u^1) \quad (56)$$

where  $a^1 = 0.25$ ,  $a^2 = 2$ ,  $a^3 = 1$ ,  $a^4 = 3.4$ , and the diffusivity matrices are constant, isotropic  $D^1 = D^2 = 0.01\mathbf{I}_2$  and  $\mathbf{I}_2$  is the  $2 \times 2$  identity matrix. The computational domain is the two-dimensional unit square  $\Omega = [-0.5, 0.5] \times [-0.5, 0.5]$  with the prey initially uniformly distributed, and predators initially gathered near  $(x_0, y_0) = (-0.25, -0.25)$

$$u^1(x, y, 0) = 1.0 \quad \text{and} \quad u^2(x, y, 0) = \begin{cases} 0 & r > d \\ e^{-\frac{d^2}{d^2 - r^2}} & r \leq d \end{cases}, \quad (57)$$

where  $d = 0.2$ ,  $r = \sqrt{(x - x_0)^2 + (y - y_0)^2}$ . The boundary conditions are all Neumann conditions  $\frac{\partial u}{\partial n} = 0$  and the velocity fields are constant  $v^1(x) = (0, 0)$  and  $v_2(x) = (0.5, 0.5)$ . The equations are discretized with a standard high-order discontinuous Galerkin method using Roe's upwind flux [25] for the inviscid numerical flux and the Compact DG flux [26] for the viscous numerical flux on a  $40 \times 40$  structured mesh of quadratic simplex elements.

The governing equations in (55) reduce to the following system of ODEs after the DG discretization is applied

$$\mathbf{M}^i \dot{\mathbf{u}}^i = \mathbf{r}^i(\mathbf{u}^i) + \mathbf{c}^i(\mathbf{u}^1, \mathbf{u}^2), \quad (58)$$

where  $\mathbf{M}^i$  is the fixed mass matrix,  $\mathbf{u}^i(t)$  is the semi-discrete state vector, i.e., the discretization of  $u$  on  $\Omega$ ,  $\mathbf{r}^i(\mathbf{u}^i)$  is the spatial discretization of the advection and diffusion terms on  $\Omega$ , and  $\mathbf{c}^i$  is the coupling term that contains the DG discretization of the  $i$ th reaction source term in (56). This non-unique decomposition of the governing equation (55) implies that, once the high-order partitioned solver is applied, various terms of the reaction source term will be predicted. The solution of (58) using the IMEX4 scheme with strong Gauss-Seidel predictor is provided in Figure 2 using the time step size  $\Delta t = 0.1$ . The predators are diffused quickly and migrate diagonally upward, while the prey are mostly affected by the coupled reaction near the extent of the predator population.

To validate the temporal convergence of the high-order partitioned scheme, we apply the 2nd-order 2-stage trapezoidal rule, 3rd-order 4-stage ARK3(2)4L[2]SA, and 4th-order 6 stage ARK4(3)6L[2]SA [19] to the ADR system in (58). Similar to the previous section, these schemes will be abbreviated by IMEX2, IMEX3, and IMEX4, respectively. For a given IMEX-RK scheme, the four predictors proposed in Section 3.2.2 are tested. Similar to the previous section, we use the  $L_\infty$ -error between a reference solution and the numerical solution provided by a particular solver at an instant in time  $t = 1.0$  to quantify the error

$$e_{\text{ADR}} = \|\mathbf{u}^1(1.0) - \mathbf{u}_N^1\|_\infty, \quad (59)$$

where  $\mathbf{u}^1(1.0)$  is a reference solution of the first subsystem at  $t = 1.0$  obtained by using the IMEX4 scheme with  $\Delta t = 6.25 \times 10^{-3}$  and the strong Gauss-Seidel predictor and  $\mathbf{u}_N^1$  is the numerical solution at the final time step for the first subsystem. The error  $e_{\text{ADR}}$  as a function of time step size for the second, third, and fourth order IMEX-RK methods are provided in Figure 3. From this figure we see the design order of accuracy of the scheme is obtained for all four proposed predictors. Unlike the ODE system in the previous system, there is not a significant difference between the accuracy at a given time step between the Jacobi and Gauss-Seidel predictors. This figure also shows that no stability issues were observed for any of the predictors, even for the coarsest time step  $\Delta t = 0.1$ .

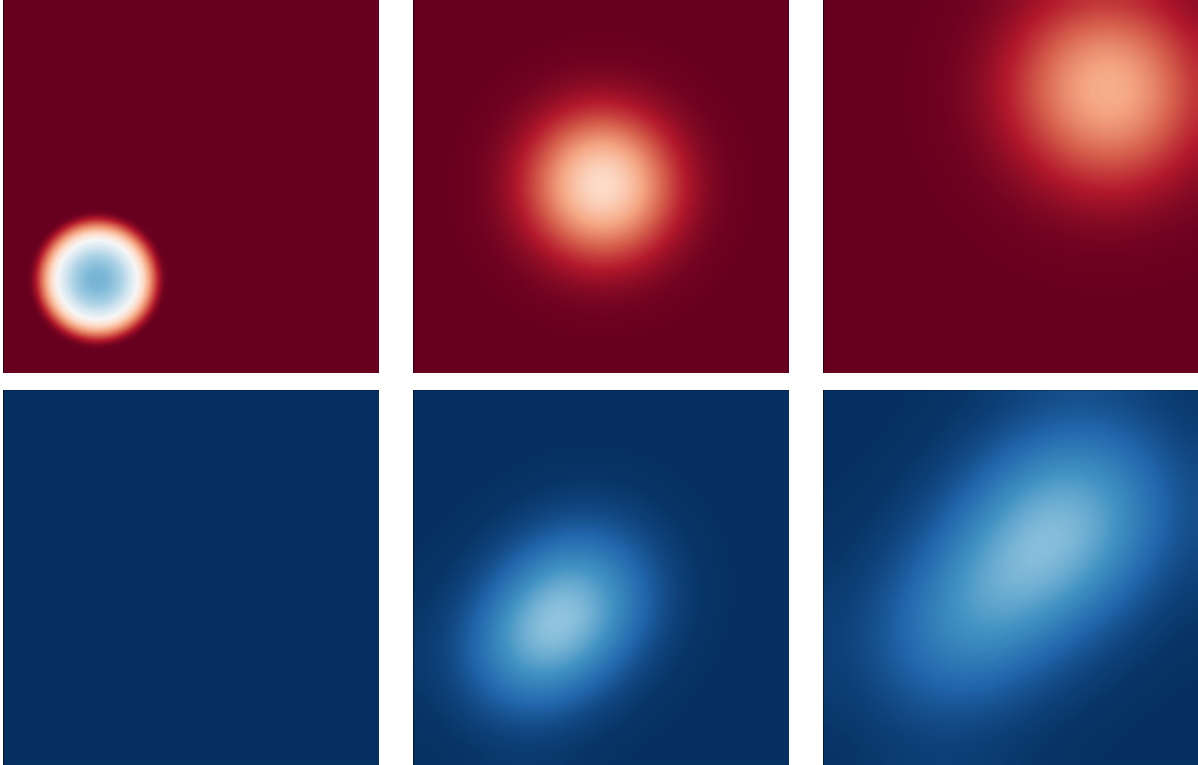


Figure 2: Predator (*top*) and prey (*bottom*) populations at various snapshots in time:  $t = 0.0$  (*left*),  $t = 0.5$  (*center*), and  $t = 1.0$  (*right*).

## 6. Application to fluid-structure interaction

In this section, we demonstrate the proposed high-order IMEX-based partitioned solver on fluid-structure interaction (FSI) problems. Partitioned solution procedures are widely used to solve such problems given that they allow maximal re-use of individual fluid and structure software. The FSI problem is usually formulated in an Arbitrary Lagrangian-Eulerian framework using three fields: the deformation of the solid, the fluid flow, and the motion of the fluid mesh. The deformation of the fluid mesh is commonly assumed quasi-static [27, 28] or interpolation, e.g., via radial basis functions, is used to transfer the boundary displacement of the fluid mesh into the interior [16, 17]. In both cases, the formulation effectively reduces to a two-field system involving the structural displacements and the fluid flow. Both two- and three-field FSI formulations are considered in this section.

### 6.1. Governing equations and semi-discretization

This section introduces the governing partial differential equations for the 2- and 3-field FSI formulation as a coupled multiphysics system (1) and their semi-discretization to yield a system of ODEs connected via coupling terms (3).

#### 6.1.1. Compressible fluid flow

The governing equations for compressible fluid flow, defined on a deformable fluid domain  $\Omega(t)$ , can be written as a viscous conservation law

$$\frac{\partial U}{\partial t} + \nabla \cdot \mathcal{F}^{inv}(U) + \nabla \cdot \mathcal{F}^{vis}(U, \nabla U) = 0 \quad \text{in } \Omega(t), \quad (60)$$

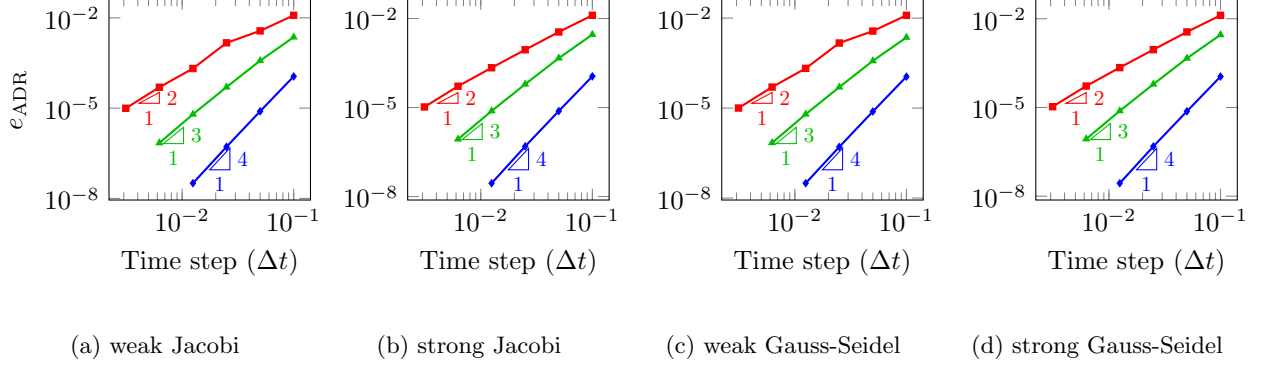


Figure 3: Convergence of the IMEX2 (—■—), IMEX3 (—▲—), and IMEX4(—◆—) schemes with various predictors applied to the predator-prey ADR system. For this problem, all predictors achieve the design order of the IMEX schemes, with small differences in the accuracy.

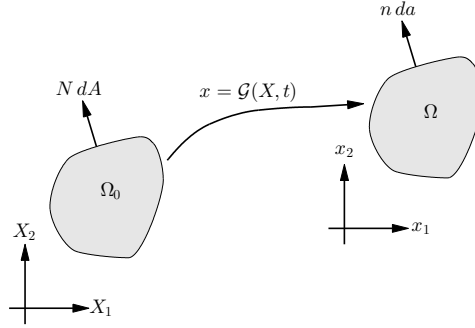


Figure 4: Mapping between reference and physical domains.

where  $U$  is the conservative state variable vector and the physical flux consists of inviscid part  $\mathcal{F}^{inv}(U)$  and a viscous part  $\mathcal{F}^{vis}(U, \nabla U)$ . The conservation law in (60) is transformed to a fixed reference domain  $\Omega_0$  by defining a time-dependent diffeomorphism  $\mathcal{G}$  between the reference domain and physical domain; see Figure 4. At each time  $t$ , a point  $X$  in the reference domain  $\Omega_0$  is mapped to  $x(X, t) = \mathcal{G}(X, t)$  in the physical domain  $\Omega(t)$ . The deformation gradient  $G$ , velocity  $v_G$ , and Jacobian  $g$  of the mapping are defined as

$$G = \nabla_X \mathcal{G}, \quad v_G = \frac{\partial \mathcal{G}}{\partial t}, \quad g = \det G. \quad (61)$$

Following the procedure in [29, 30], the governing equation (60) can be written in the reference domain as

$$\frac{\partial U_X}{\partial t} + \nabla_X \cdot \mathcal{F}_X^{inv}(U_X) + \nabla_X \cdot \mathcal{F}_X^{vis}(U_X, \nabla_X U_X) = 0 \quad \text{in } \Omega_0, \quad (62)$$

where  $\nabla_X$  defines the spatial derivative with respect to the reference domain, conserved quantities and its derivatives in the reference domain are written as

$$U_X = gU, \quad \nabla_X U_X = g \nabla U_X \cdot G + g^{-1} U_X \frac{\partial g}{\partial X}. \quad (63)$$

The inviscid and viscous fluxes are transformed to the reference domain as

$$\begin{aligned} \mathcal{F}_X^{inv}(U_X) &= g \mathcal{F}^{inv}(g^{-1} U_X) G^{-T} - U_X \otimes G^{-1} v_G, \\ \mathcal{F}_X^{vis}(U_X) &= g \mathcal{F}^{vis} \left( g^{-1} U_X, g^{-1} \left[ \nabla_X U_X - g^{-1} U_X \frac{\partial g}{\partial X} \right] G^{-1} \right) G^{-T}. \end{aligned} \quad (64)$$

The governing equations in (62) reduce to the following system of ODEs after an appropriate spatial discretization, such as a discontinuous Galerkin or finite volume method, is applied

$$\mathbf{M}^f \dot{\mathbf{u}}^f = \mathbf{r}^f(\mathbf{u}^f, \mathbf{c}^f), \quad (65)$$

where  $\mathbf{M}^f$  is the fixed mass matrix,  $\mathbf{u}^f(t)$  is the semi-discrete fluid state vector, i.e., the discretization of  $U_X$  on  $\Omega_0$ ,  $\mathbf{r}^f(\mathbf{u}^f, \mathbf{c}^f)$  is the spatial discretization of the transformed inviscid and viscous fluxes on  $\Omega_0$ , and  $\mathbf{c}^f$  is the coupling term that contains information about the domain mapping  $\mathcal{G}(X, t)$ . In particular, the coupling term contains the position and velocities of the nodal coordinates of the computational mesh. The domain mapping is defined using an element-wise nodal (Lagrangian) polynomial basis on the mesh with coefficients from the nodal positions and velocities.

### 6.1.2. Simple structure model

In general, the governing equations for the structure will be given by a system of partial differential equation such as the continuum equations in total Lagrangian form with an arbitrary constitutive law. However, in this work, we only consider simple structures such as mass-spring-damper systems that can directly be written as a second-order system of ODEs

$$m_s \ddot{u}_s + c_s \dot{u}_s + k_s u_s = f_{ext}(t), \quad (66)$$

where  $m_s$  is the mass of the (rigid) object,  $c_s$  is the damper resistance constant,  $k_s$  is the spring stiffness, and  $f_{ext}(t)$  is a time-dependent external load, which will be given by integrating the pointwise force the fluid exerts on the object. These simple structures allow us to study the stability and accuracy properties of the proposed high-order partitioned solver for this class of multiphysics problems without the distraction of transferring solution fields across the fluid-structure interface.

To conform to the notation in this document and encapsulate the semi-discretization of PDE-based structure models, the equations in (66) are re-written in a first-order form as

$$\mathbf{M}^s \dot{\mathbf{u}}^s = \mathbf{r}^s(\mathbf{u}^s, \mathbf{c}^s). \quad (67)$$

In the case of the simple structure in (66), the mass matrix, state vector, residual, and coupling term are

$$\mathbf{M}^s = \begin{bmatrix} m_s & \\ & 1 \end{bmatrix}, \quad \mathbf{u}^s = \begin{bmatrix} \dot{u}_s \\ u_s \end{bmatrix}, \quad \mathbf{c}^s = f_{ext}, \quad \mathbf{r}^s(\mathbf{u}^s, \mathbf{c}^s) = \begin{bmatrix} f_{ext} - c_s \dot{u}_s - k_s u_s \\ u_s \end{bmatrix}. \quad (68)$$

### 6.1.3. Deformation of the fluid domain

In the three-field fluid-structure interaction formulation pioneered in [27, 28], the fluid mesh is considered a pseudo-structure driven solely by Dirichlet boundary conditions provided by the displacement of the structure at the fluid-structure interface. The governing equations are given by the continuum mechanics equations in total Lagrangian form with an arbitrary constitutive law

$$\begin{aligned} \frac{\partial \bar{p}}{\partial t} - \nabla \cdot P(G) &= 0 && \text{in } \Omega_0 \\ x &= x_b && \text{on } \partial\Omega_0^D \\ \dot{x} &= \dot{x}_b && \text{on } \partial\Omega_0^D, \end{aligned} \quad (69)$$

where  $\bar{p}(X, t) = \rho_m \dot{x}$  is the linear momentum,  $\rho_m$  is the density, and  $P$  is the first Piola-Kirchhoff stress of the pseudo-structure. The deformation gradient  $G$  is the mapping that defines the deformation of the reference fluid domain  $\Omega_0$  to physical fluid domain  $\Omega(t)$ . The position and velocity of the fluid domain are prescribed along  $\partial\Omega_0^D$ , the union of the fluid-structure interface and the fluid domain boundary.

The governing equations in (69) reduce to the following system of ODEs after an appropriate spatial

discretization, such as the finite element method, is applied and recast in first-order form

$$\mathbf{M}^x \dot{\mathbf{u}}^x = \mathbf{r}^x(\mathbf{u}^x, \mathbf{c}^x) \quad (70)$$

where  $\mathbf{M}^x$  is the fixed mass matrix,  $\mathbf{u}^x(t)$  is the semi-discrete state vector consisting of the displacements and velocities of the mesh nodes,  $\mathbf{r}^x(\mathbf{u}^x, \mathbf{c}^x)$  is the spatial discretization of the continuum equations and boundary conditions on the reference domain  $\Omega_0$ , and  $\mathbf{c}^x$  is the coupling term that contains information about the motion of the fluid structure interface. This model of the mesh motion leads to a three-field FSI formulation when coupled to the fluid and structure equations.

Alternatively, the motion of the fluid mesh can be described through a parametrized mapping such as radial basis functions [16, 31, 17] or blending maps [29]. That is, the domain mapping  $x = \mathcal{G}(X, t)$  is given by an analytical function, parametrized by the deformation and velocity of the fluid-structure interface, that can be analytically differentiated to obtain the deformation gradient  $G(X, t)$  and velocity  $v_G(X, t)$ . Since the fluid mesh motion is no longer included in the system of time-dependent partial differential equations, this leads to a two-field FSI formulation in terms of the fluid and structure states only.

#### 6.1.4. Two-field and three-field fluid-structure coupling

In the three-field fluid-structure interaction setting

$$\mathbf{M}^s \dot{\mathbf{u}}^s = \mathbf{r}^s(\mathbf{u}^s, \mathbf{c}^s), \quad \mathbf{M}^x \dot{\mathbf{u}}^x = \mathbf{r}^x(\mathbf{u}^x, \mathbf{c}^x), \quad \mathbf{M}^f \dot{\mathbf{u}}^f = \mathbf{r}^f(\mathbf{u}^f, \mathbf{c}^f) \quad (71)$$

introduced in [27], the coupling terms have the following dependencies

$$\mathbf{c}^s = \mathbf{c}^s(\mathbf{u}^s, \mathbf{u}^x, \mathbf{u}^f), \quad \mathbf{c}^x = \mathbf{c}^x(\mathbf{u}^s), \quad \mathbf{c}^f = \mathbf{c}^f(\mathbf{u}^s, \mathbf{u}^x). \quad (72)$$

From Eq. (68), the structure coupling term is the external force applied to the structure that comes from integrating the fluid stresses over the fluid-structure interface. The mesh coupling term is the position and velocity of the fluid-structure interface and therefore depends solely on the state of the structure. From Eq. (62)-(63), the fluid coupling term is the position and velocity of the entire fluid mesh and therefore depends on the state of the structure and the mesh.

In the two-field FSI setting

$$\mathbf{M}^s \dot{\mathbf{u}}^s = \mathbf{r}^s(\mathbf{u}^s, \mathbf{c}^s), \quad \mathbf{M}^f \dot{\mathbf{u}}^f = \mathbf{r}^f(\mathbf{u}^f, \mathbf{c}^f) \quad (73)$$

the mesh motion is given by an analytical function and the coupling terms have the following dependencies

$$\mathbf{c}^s = \mathbf{c}^s(\mathbf{u}^s, \mathbf{u}^f), \quad \mathbf{c}^f = \mathbf{c}^f(\mathbf{u}^s). \quad (74)$$

In this case, the structure coupling term is determined from the fluid and structure state since the external force depends on the traction integrated over the fluid-structure interface. The fluid coupling term, i.e., the position and velocity of the fluid mesh, is determined from the structure state. Finally, the ordering of the subsystems implied in (71) and (73) is used throughout the remainder of this section, which plays an important role when defining the Gauss-Seidel predictors.

#### 6.2. 1D Fluid-structure-mesh three-field coupling piston problem

We begin our investigation into the performance of the proposed high-order, partitioned multiphysics solver in the FSI context with the canonical FSI model problem: a one-dimensional piston (Figure 5). The

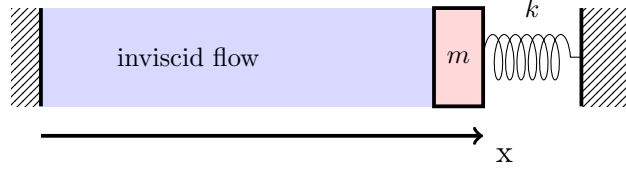


Figure 5: One-dimensional piston system

inviscid fluid is governed by the one-dimensional Euler equations

$$\begin{aligned}
 \frac{\partial \rho}{\partial t} + \frac{\partial \rho u}{\partial x} &= 0 \\
 \frac{\partial \rho u}{\partial t} + \frac{\partial (\rho u^2 + p)}{\partial x} &= 0 \\
 \frac{\partial \rho E}{\partial t} + \frac{\partial (u(\rho E + p))}{\partial x} &= 0
 \end{aligned} \tag{75}$$

for  $x \in \Omega(t) = [0, 1.0 - u_s]$ , where  $u_s$  is the displacement of the piston,  $\rho$  is the fluid density,  $u$  is the fluid velocity,  $E$  is the total energy, the pressure  $p$  is given by the ideal gas law

$$p = (\gamma - 1)\rho\left(E - \frac{1}{2}u^2\right), \tag{76}$$

and the adiabatic gas constant is  $\gamma = 1.4$ . The fluid is initially at rest  $u = 0$  with a density  $\rho = 1.0$  and pressure  $p = 0.4$ . After transformation to the reference domain  $\Omega_0 = [0, 1]$  following the procedure in Section 6.1.1, the equations are semi-discretized by a standard first-order finite volume method using Roe's flux [25] with 128 elements.

The deformation of the fluid mesh is handled by considering the fluid domain to be a pseudo-structure governed by the continuum equations in Eq. (69), restricted to the one-dimensional case with a linear, isotropic constitutive law and infinitesimal strains assumed

$$\rho_m \ddot{u}_x = E_m \frac{\partial^2 u_x}{\partial X^2} - c_m \dot{u}_x, \tag{77}$$

where  $u_x(X, t)$  is the mesh displacement vector defined over the reference domain  $X \in \Omega_0$  and the density, Young's modulus, and damping coefficient are  $\rho_m = 1.0$ ,  $E_m = 1.0$ ,  $c_m = 0.0$ , respectively. The governing equation for the mesh deformation is discretized in space using the finite difference method.

Finally, the structure is modeled by a linear mass-spring system as Eq. (66) with piston mass  $m_s = 1.0$ , spring stiffness  $k_s = 1.0$ , and no damper  $c_s = 0$ . The piston is initially displaced a distance of  $u_s = -0.3$ . Once the piston is released, it immediately begins to recede due to the combination of the spring being perturbed from its equilibrium configuration and the flow pressure, which causes a  $C^0$  rarefaction wave near the interface.

To validate the temporal convergence of the scheme, the proposed high-order partitioned framework is applied to solve the three-field coupled FSI problem. In this case, we only consider the weak and strong Gauss-Seidel predictors. The accuracy of a given simulation is quantified by considering the error in fluid, mesh, and structure states between a reference solution and the numerical solution at time  $t = 5.0$

$$\begin{aligned}
 e_{\text{FSI3}}^f &= \left\| \mathbf{u}_N^f - \mathbf{u}^f(5.0) \right\|_{\infty} \\
 e_{\text{FSI3}}^x &= \left\| \mathbf{u}_N^x - \mathbf{u}^x(5.0) \right\|_{\infty} \\
 e_{\text{FSI3}}^s &= \left\| \mathbf{u}_N^s - \mathbf{u}^s(5.0) \right\|_{\infty},
 \end{aligned} \tag{78}$$

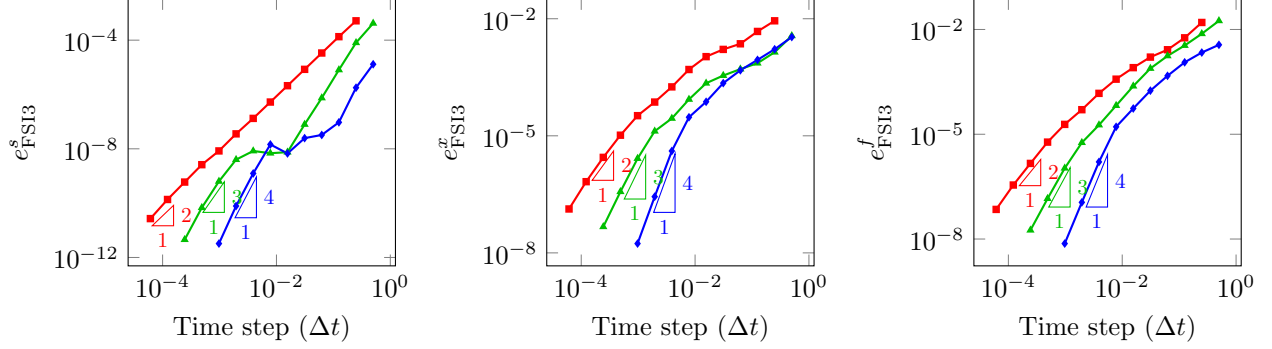


Figure 6: Convergence of the IMEX2 (—■), IMEX3 (—▲), and IMEX4 (—◆) with the **weak** Gauss-Seidel predictor as applied to the three-field coupling piston problem.

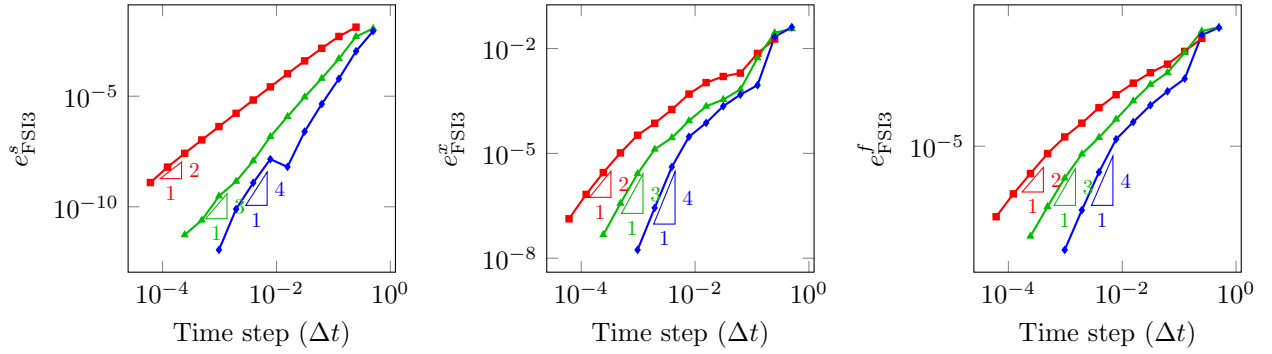


Figure 7: Convergence of the IMEX2 (—■), IMEX3 (—▲), and IMEX4 (—◆) with the **strong** Gauss-Seidel predictor as applied to the three-field coupling piston problem.

where  $\mathbf{u}^f(5.0)$ ,  $\mathbf{u}^x(5.0)$ ,  $\mathbf{u}^s(5.0)$  are the fluid, mesh, and structure states, respectively, from the reference solution, computed by using the IMEX4 scheme with  $\Delta t = 9.765625 \times 10^{-5}$  and strong Gauss-Seidel predictor at  $t = 5.0$  and  $\mathbf{u}_N^f$ ,  $\mathbf{u}_N^x$ ,  $\mathbf{u}_N^s$  are the corresponding states from the numerical solution at the final time step. The convergence plots are provided in Figure 6 and Figure 7 and show the partitioned solver with both predictors attain the design order of accuracy of the IMEX-RK scheme, despite the fact that the solution is not  $C^1$  continuous due to the rarefaction wave.

### 6.3. 2D Fluid-structure two-field coupling foil damper problem

We continue our investigation into the performance of the proposed high-order, partitioned multiphysics solvers on FSI problems with a two-dimensional energy-harvesting model problem [32, 30] that uses a two-field FSI formulation. Consider the mass-damper system in Figure 8 suspended in an isentropic, viscous flow where the rotational motion is a prescribed periodic motion  $\theta(t) = \frac{\pi}{4} \cos(2\pi ft)$  with frequency  $f = 0.2$  and the vertical displacement is determined by balancing the forces exerted on the airfoil by fluid and damper. The governing equations for the fluid are the isentropic Navier-Stokes equations:

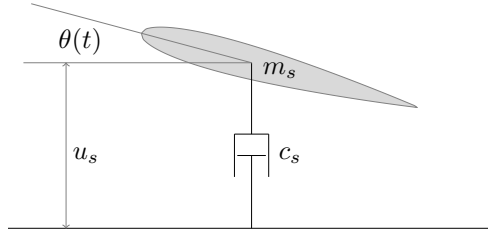


Figure 8: Foil-damper system

$$\frac{\partial \rho}{\partial t} + \frac{\partial}{\partial x_i}(\rho u_i) = 0, \quad (79)$$

$$\frac{\partial}{\partial t}(\rho u_i) + \frac{\partial}{\partial x_i}(\rho u_i u_j + p) = + \frac{\partial \tau_{ij}}{\partial x_j} \quad \text{for } i = 1, 2, 3, \quad (80)$$

$$\frac{\partial}{\partial t}(\rho E) + \frac{\partial}{\partial x_i}(u_j(\rho E + p)) = - \frac{\partial q_j}{\partial x_j} + \frac{\partial}{\partial x_j}(u_j \tau_{ij}), \quad (81)$$

in  $\Omega(t)$  where  $\rho$  is the fluid density,  $u_1, u_2, u_3$  are the velocity components, and  $E$  is the total energy. The viscous stress tensor and heat flux are given by

$$\tau_{ij} = \mu \left( \frac{\partial u_i}{\partial x_j} + \frac{\partial u_j}{\partial x_i} - \frac{2}{3} \frac{\partial u_k}{\partial x_k} \delta_{ij} \right) \quad \text{and} \quad q_j = - \frac{\mu}{\text{Pr}} \frac{\partial}{\partial x_j} \left( E + \frac{p}{\rho} - \frac{1}{2} u_k u_k \right).$$

Here,  $\mu$  is the viscosity coefficient and  $\text{Pr} = 0.72$  is the Prandtl number which we assume to be constant. For an ideal gas, the pressure  $p$  has the form

$$p = (\gamma - 1) \rho \left( E - \frac{1}{2} u_k u_k \right), \quad (82)$$

where  $\gamma$  is the adiabatic gas constant. The isentropic assumption states the entropy of the system is assumed constant, which is tantamount to the flow being adiabatic and reversible. For a perfect gas, the entropy is defined as

$$s = p / \rho^\gamma. \quad (83)$$

The conservation law defined in (79)-(81) is reformulated in an ALE framework, i.e., transformed to a reference domain  $\Omega_0$ , as described in Section 6.1.1. The transformed conservation law is discretized with a standard high-order discontinuous Galerkin method using Roe's flux [25] for the inviscid numerical flux and the Compact DG flux [26] for the viscous numerical flux. The DG discretization uses a mesh consisting of 3912 cubic simplex elements. The second-order ODE in Eq. (66) is the governing equation for the mass-damper system with mass  $m_s$ , damping constant  $c_s = 1$ , stiffness  $k_s = 0$ , and external force given from the fluid as described in Section 6.1.2. The mesh motion is determined from the position and velocity of the structure using the blending maps introduced in [29] and identical to that used in Section 5.1 of [30]. Snapshots of the vorticity field and motion of the airfoil are shown in Figure 9 for a single configuration of the fluid-structure system.

Our first numerical experiment studies the stability of the four proposed predictors as a function of the mass ratio between the structure and fluid, an important parameter that can impact the stability of partitioned solvers as identified in [13, 16], and time step size for IMEX schemes up to fourth order. The mass ratio,  $\bar{m}$ , considered is the ratio of the mass of the structure,  $m$ , to the mass of fluid displaced by the structure,  $\rho A$ , where  $\rho$  is the density of the fluid and  $A = 0.08221$  is the area of the airfoil. Since the isentropic Navier-

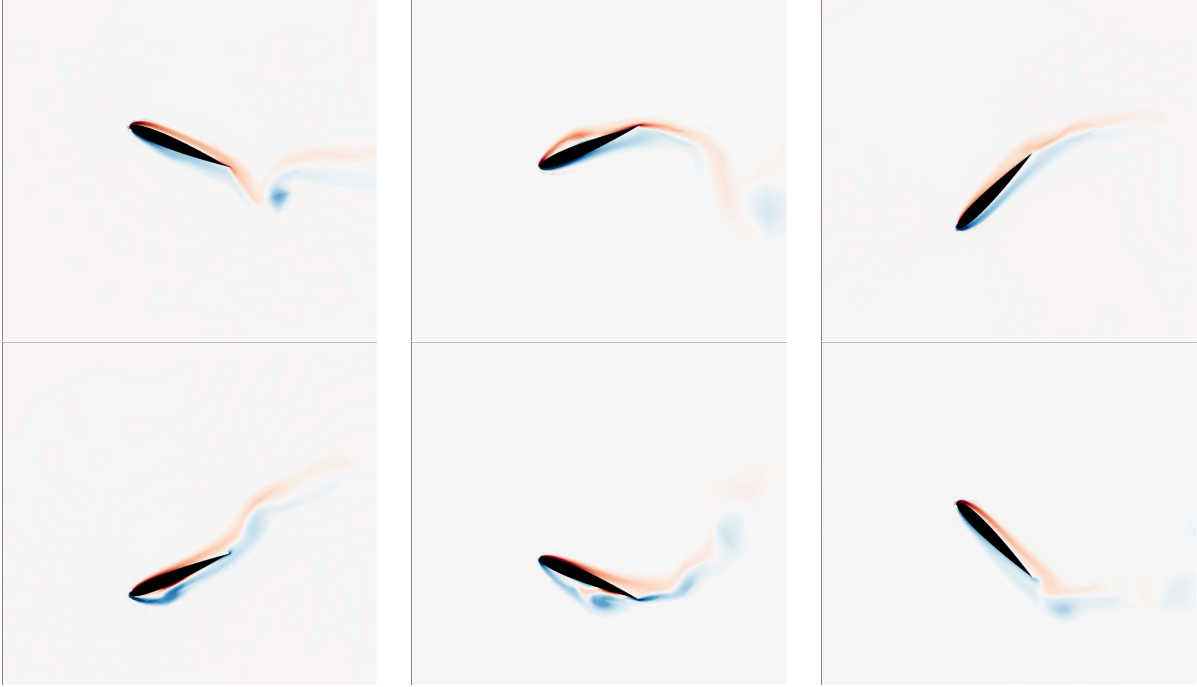


Figure 9: Airfoil motion and flow vorticity corresponding to foil-damper system under prescribed rotational motion  $\theta(t) = \frac{\pi}{4} \cos(2\pi ft)$  with frequency  $f = 0.2$  at various snapshots in time:  $t = 0.83, 1.67, 2.5, 3.33, 4.17, 5.0$  (left-to-right, top-to-bottom).

Stokes equations can be seen as an artificial compressibility formulation for the incompressible Navier-Stokes equations [33, 34], we consider the density to be constant and equal to the freestream  $\rho = 1$ . Variations in the mass ratio are achieved by varying the mass of the structure with all other parameters fixed. The stability results are summarized in Figure 10 where  $\blacktriangle$  indicates a  $(\Delta t, \bar{m})$ -pair that leads to a stable simulation and  $\blacksquare$  leads to an unstable one. This figure shows the weak and strong Jacobi predictors lack robustness beyond the first-order scheme since they only lead to stable simulations for small step sizes or large mass ratios, while the Gauss-Seidel predictors are stable across a larger set of  $(\Delta t, \bar{m})$  pairs. This does not contradict the stability theory in Section 3.2.4 since the robustness issues manifest as a nonlinear instabilities that come from lagging the mesh motion to the previous time step during the fluid solve. Figure 10 also shows that all schemes are stable once the time step is sufficiently small, at least for this range of mass ratios considered. The first-order IMEX scheme is the most robust, which is expected given the large amount of numerical dissipation associated with first-order solvers. This figure also highlights the robustness of the proposed solver, particularly with the Gauss-Seidel predictor, since the maximum stable time step is three orders of magnitude larger than the maximum stable time step of a fluid-only simulation with RK4, indicating the scheme benefits from treating both subsystems implicitly and the coupling correction explicitly.

With the stability of the predictors established, we confirm the order of accuracy for the Gauss-Seidel predictors in Figure 11 up to fourth order. The error metric used is the error in the time-integrated vertical force the fluid exerts on the structure, i.e., the integral of the fluid stress tensor over the airfoil over time, denoted  $e_{\text{FSI2}}$ . The temporal integral is computed to exactly the same order as the semi-discrete system by recasting the time integral to an ODE and applying the same IMEX scheme, i.e., solver-consistent integration of quantities of interest [30]. A reference solution is computed using the IMEX5 scheme with  $\Delta t = 3.125 \times 10^{-3}$  and strong Gauss-Seidel predictor.

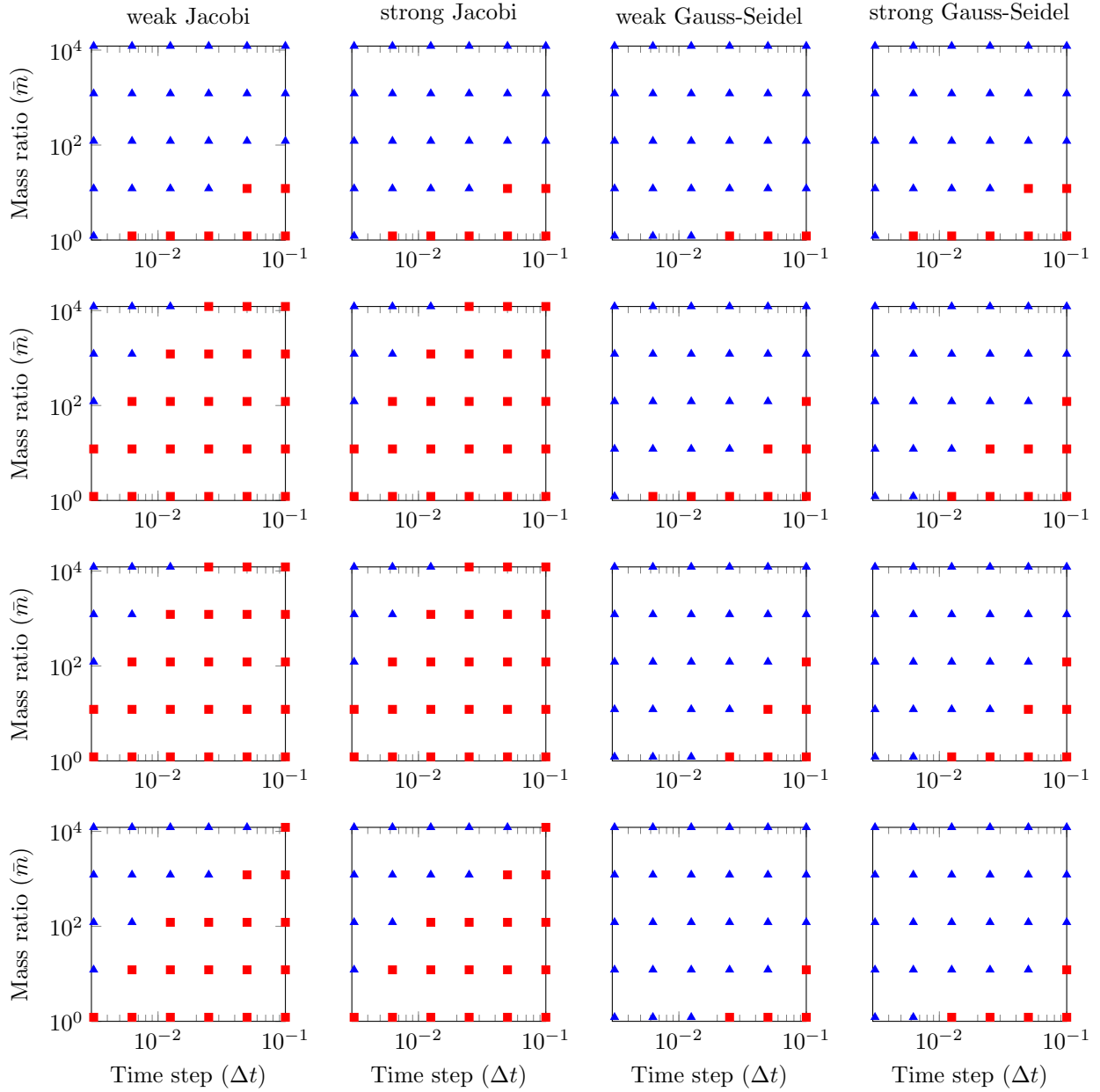


Figure 10: Behavior of the predictor-based partitioned schemes for a range of mass ratios and time steps for IMEX1-IMEX4 (top to bottom) schemes with the weak Jacobi predictor (left), strong Jacobi predictor (center left), weak Gauss-Seidel predictor (center right), and strong Gauss-Seidel predictor (right). Legend:  $\blacktriangle$  indicates a stable simulation and  $\blacksquare$  indicates an unstable simulation.

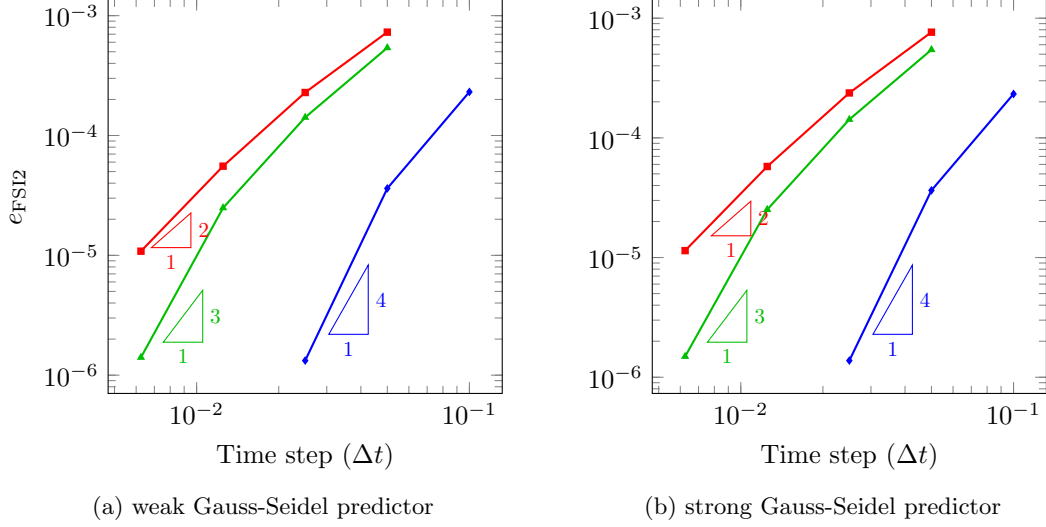


Figure 11: Convergence of the IMEX2 (—■—), IMEX3 (—▲—), and IMEX4 (—◆—) with Gauss-Seidel type predictors as applied to the foil-damper system. Both predictors achieve the design orders and give very similar levels of accuracy.

## 7. Application to particle-laden flows

Our final application is a two-phase particle-laden flow that is common in biological flows [35], plasma problems [36], and environmental flows [37], among others. In these flows, momentum and energy are exchanged between the carrier flow and small, immiscible particles. This interaction plays an important role in both phases of the flow and results in complex behavior.

The governing equations for the carrier flow are the unsteady compressible Navier-Stokes equations (60) with a source term that accounts for the momentum and energy the particles contribute to the flow

$$\begin{aligned}
\frac{\partial \rho}{\partial t} + \frac{\partial}{\partial x_i}(\rho u_i) &= 0, \\
\frac{\partial}{\partial t}(\rho u_i) + \frac{\partial}{\partial x_i}(\rho u_i u_j + p) &= f_i + \frac{\partial \tau_{ij}}{\partial x_j} \quad \text{for } i = 1, 2, \dots, d, \\
\frac{\partial}{\partial t}(\rho E) + \frac{\partial}{\partial x_i}(u_j(\rho E + p)) &= f_j u_j - \frac{\partial q_j}{\partial x_j} + \frac{\partial}{\partial x_j}(u_j \tau_{ij}),
\end{aligned} \tag{84}$$

in the spatial-temporal domain  $(x, t) \in \Omega \times (0, T]$ , where  $f = [f_1 \ \dots \ f_d]^T$  is the force the particles exert on the flow and all quantities are defined in (79)-(82). The force a system of  $M$  particles at positions  $x_1, \dots, x_M$  with velocities  $v_1, \dots, v_M$  exert on the fluid at a position  $x$  is approximated as

$$f(x) = - \sum_{k=1}^M m_p \frac{u - v_k}{\tau_p} D(\|x - x_k\|_2), \tag{85}$$

where  $m_p$  and  $\tau_p$  are the mass and response time of the particle, and  $D(r)$  is an approximated Dirac delta function

$$D(r) = \frac{1}{(2\pi\sigma^2)^{d/2}} \exp\left(-\frac{r^2}{2\sigma^2}\right). \tag{86}$$

For particles of diameter  $d_p$  and density  $\rho_p$ , Stokes' drag law gives the following relation for the particle response time

$$\tau_p = \frac{d_p^2 \rho_p}{18\mu}, \tag{87}$$



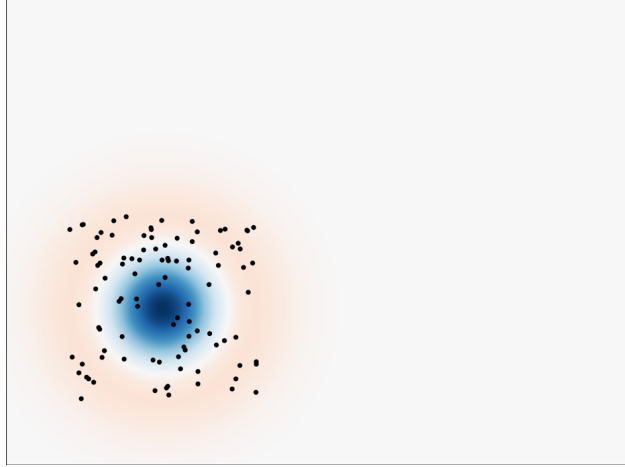


Figure 12: Vorticity profile and particles at  $t = 0$

numerical flux on a structured mesh of 2400 simplex elements. After the DG spatial discretization is applied, the governing equations reduce to the following system of ODEs

$$\mathbf{M}^f \dot{\mathbf{u}}^f = \mathbf{r}^f(\mathbf{u}^f, \mathbf{c}^f(\mathbf{q})) \quad (93)$$

where  $\mathbf{M}^f$  is the fixed mass matrix,  $\mathbf{u}^f(t)$  is the semi-discrete state vector, i.e., the discretization of  $U$  on  $\Omega$ ,  $\mathbf{r}^f(\mathbf{u}^f)$  is the spatial discretization of the inviscid and viscous flux terms on  $\Omega$ , and  $\mathbf{c}^f = \mathbf{q}$  is the coupling term.

Given the extensive studies of the order of accuracy of the four predictors in the previous section, we focus this section on stability of the weak and strong Gauss-Seidel predictors. In the following numerical experiments, the solution is integrated to time  $t = 10.0$  with time step  $\Delta t = 0.1$ , regardless of the IMEX-RK scheme used. Since the particle-laden flow is a two-system multiphysics problem, the coupling structure conforms to the format in Eq. (35) and only one coupling predictor is required:  $\tilde{\mathbf{c}}^q$ . The weak Gauss-Seidel predictor lags the fluid velocity and particle state to the previous time step

$$\tilde{\mathbf{c}}^q(\mathbf{q}, \mathbf{u}^f, \bar{\mathbf{q}}, \bar{\mathbf{u}}^f) = [\bar{u}(\bar{x}_1)^T \quad \dots \quad \bar{u}(\bar{x}_M)^T]^T, \quad (94)$$

while the strong Gauss-Seidel lags the fluid velocity to the current time step, but uses the current particle state

$$\tilde{\mathbf{c}}^q(\mathbf{q}, \mathbf{u}^f, \bar{\mathbf{q}}, \bar{\mathbf{u}}^f) = [\bar{u}(x_1)^T \quad \dots \quad \bar{u}(x_M)^T]^T. \quad (95)$$

We consider two scenarios: (1) light particles:  $\rho_p = 0.1$ ,  $d_p = 0.01$  and (2) heavy particles:  $\rho_p = 1000.0$ ,  $d_p = 0.01$ . In the first case, the particle mass is about  $5.2 \times 10^{-8}$  and particle response time is about  $1.1 \times 10^{-4}$  so the coupled system is stiff considering the large coefficients in Eq. (88). Several simulations with a third-order DG discretization (quadratic  $p = 2$  elements) with different time steps are performed to demonstrate the stability of the proposed high-order partitioned solver and predictors. Figure 13a shows the particle trajectories for both weakly and strongly coupled Gauss-Seidel predictors using the second-order temporal discretization (IMEX2) with  $\Delta t = 0.1$ . In this extreme case, the weak Gauss-Seidel predictor exhibits a form of instability, which can be seen from the oscillations that appear in some particle trajectories (Figure 13a); however, the strong Gauss-Seidel predictor gives smooth results. For smaller time steps, i.e.,  $\Delta t = 0.05$ , the IMEX2 scheme with the weakly coupled Gauss-Seidel predictor leads to stable results. Interestingly, the IMEX3 and IMEX4 schemes do not exhibit the aforementioned instabilities as both the weakly and strongly coupled Gauss-Seidel predictors are stable even with larger time steps. This case demonstrates that although the weakly coupled Gauss-Seidel predictor is inferior to strongly coupled Gauss-Seidel predictor in

some cases, both possess good stability properties considering the time step is three orders of magnitude larger than the particle response time. The particle trajectories for all these cases are provided in Figure 13b.

To close this section, a formal convergence study is conducted. The accuracy is quantified via the  $L_\infty$ -norm of the error in the flow solution at time  $t = 10.0$

$$e_{\text{PL}} = \left\| \mathbf{u}_N^f - \mathbf{u}^f(10.0) \right\|_\infty, \quad (96)$$

where  $\mathbf{u}^f(10.0)$  is the reference solution computed by using the IMEX4 scheme with  $\Delta t = 1.25 \times 10^{-2}$  and strong Gauss-Seidel predictor, and  $\mathbf{u}_N^f$  is the flow state from the numerical solution at the final time step. The convergence result is presented in Figure 14, which illustrates the partitioned solver with both Gauss-Seidel predictors achieves the design order of the underlying IMEX scheme.

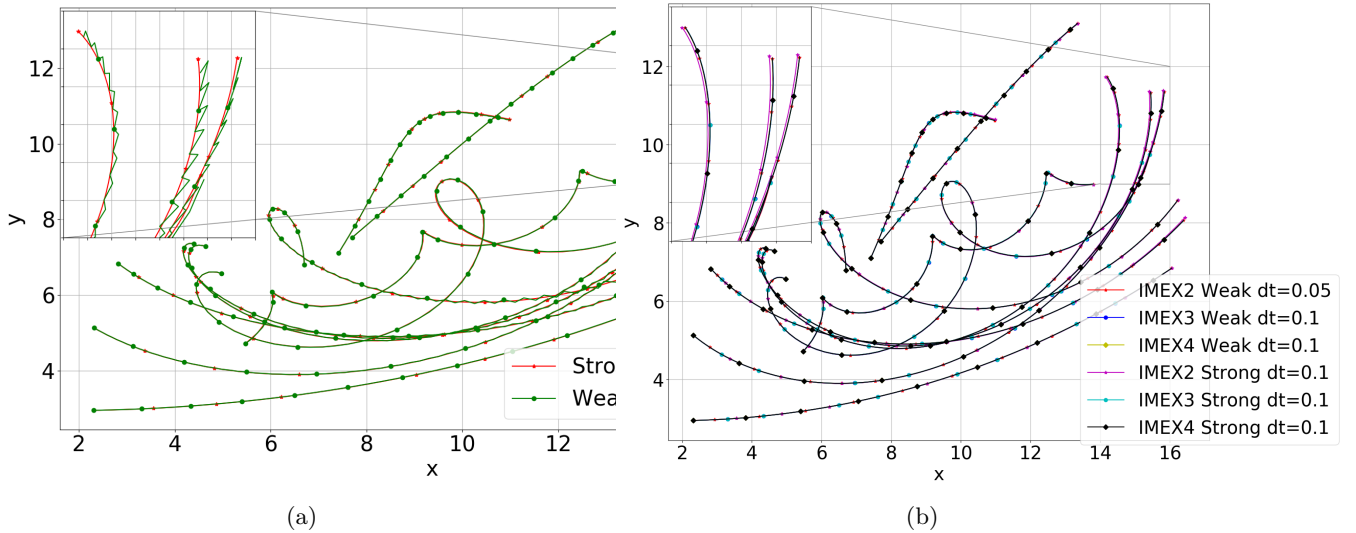


Figure 13: Sampling light particle trajectories in the unsteady compressible vortex: (a) Comparison of strong/weak GS coupling predictors for IMEX2 of  $\Delta t = 0.1$  (b) Comparison of strong/weak GS coupling predictors for different order schemes.

For the case with heavy particles, the particle mass is about  $5.2 \times 10^{-4}$  and the particle response time is about 1.11. In this case, the coupling effect is stronger than for the light particles and both predictors are stable for all discretization orders considered. Figure 15 shows the vorticity profiles and particle positions at several time instances for the simulations with light and heavy particles. Light particles drift with the vortex, while heavy particle advect with the flow since they are more affected by inertial forces.

## 8. Conclusions

This paper introduces a framework for constructing high-order, linearly stable, partitioned solvers for general multiphysics problems. The solvers are constructed from an IMEX-RK discretization applied to the monolithic system of  $n$  systems of ODEs. A specific implicit-explicit decomposition that introduces the concept of a predictor allows the monolithic systems to be solved in a partitioned manner if the predictor meets basic requirements. The four predictors, i.e., weak and strong Jacobi and Gauss-Seidel predictors, introduced lead to different IMEX-RK-based partitioned solvers, each with their own advantages and disadvantages. The weak predictors require the least implementation effort since they do not require any terms from the Jacobian of the coupling term and therefore allows for maximal re-use of existing software, while the strong predictors require the diagonal entries from the Jacobian of the coupling term, which is unlikely to be available in existing software. The Jacobi predictors allow for all subsystems to be solved in parallel at a given

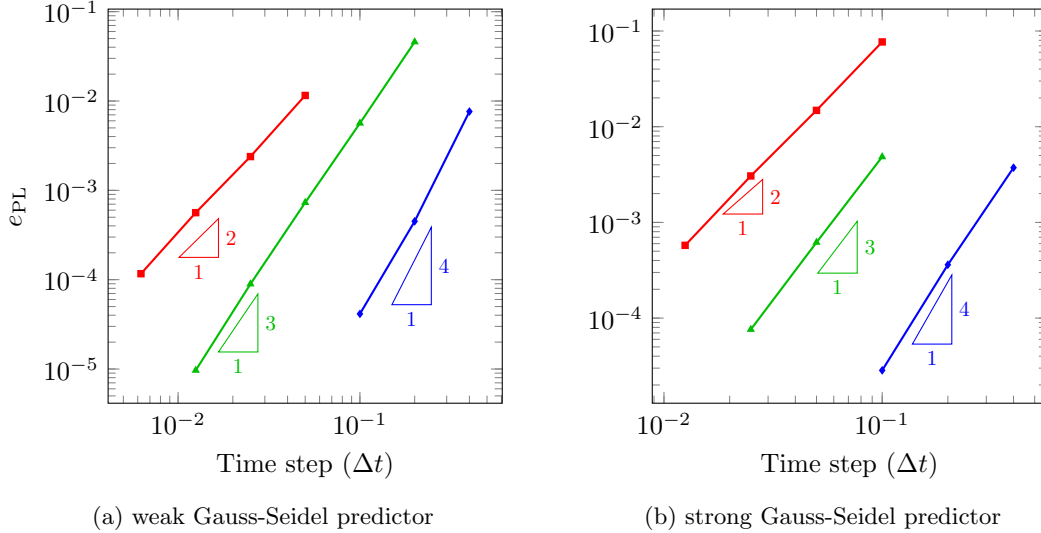


Figure 14: Convergence of the IMEX2 (—■—), IMEX3 (—▲—), and IMEX4 (—◆—) with Gauss-Seidel type predictors as applied to the particle-laden flow problem. Both predictors achieve the design orders and give very similar levels of accuracy.

stage of a given time step, while the Gauss-Seidel predictors require the subsystems be solved sequentially. Despite the simplicity and efficiency of the weak and Jacobi predictors over the strong and Gauss-Seidel predictors, they have weaker linear stability properties, which is shown theoretically and experimentally. It is interesting to note that our linear stability analysis suggests the strong Gauss-Seidel predictor is unconditionally linearly stable in the context of the chosen model problem, despite being a partitioned scheme. The performance of the four partitioned solvers was demonstrated on a slew of multiphysics problems, including an advection-diffusion-reaction system, fluid-structure interaction problems, and particle-laden flow, where we verified the design order of the IMEX scheme and studied various stability properties. Future work will consider analysis of the nonlinear stability of these schemes and derivation of the fully discrete sensitivity and adjoint equations corresponding to these four solvers so they can be used for gradient-based optimization of multiphysics systems.

## Acknowledgments

This work was supported in part by the Luis W. Alvarez Postdoctoral Fellowship (MZ), by the Director, Office of Science, Office of Advanced Scientific Computing Research, U.S. Department of Energy under Contract No. DE-AC02-05CH11231 (MZ, PP), and by the NASA National Aeronautics and Space Administration under grant number NNX16AP15A (MZ, PP). The content of this publication does not necessarily reflect the position or policy of any of these supporters, and no official endorsement should be inferred.

## Appendix A. Stability analysis of high-order, partitioned IMEX-RK solvers

In this section, we analyze the linear stability of the high-order IMEX-RK schemes: 2nd-order 2-stage trapezoidal rule, 3rd-order 4-stage ARK3(2)4L[2]SA, and 4th-order 6 stage ARK4(3)6L[2]SA [19] based on the model problem in (38) and the predictor-based implicit-explicit partitions in Table 2.

The linear stability analysis of the high-order IMEX-RK schemes proceeds according to the procedure outlined in Section 3.2.4, namely, the IMEX-RK scheme is written as a one-step update scheme (42) and region where the spectral radius of the update matrix,  $\rho(\mathbf{C})$ , is less than unity is identified. For brevity, we directly write the spectral radius and subsequently identify stable regions.

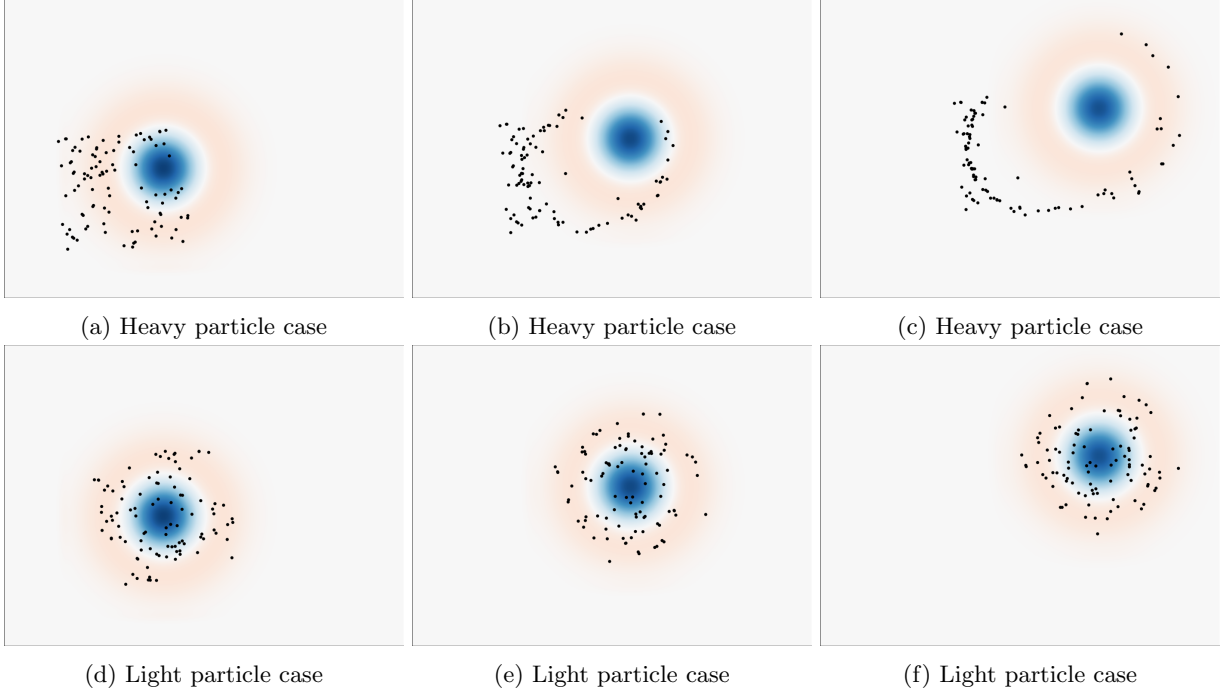


Figure 15: Particle laden flow — vorticity profiles and particle positions at  $t = 3.33, 6.67, 10$ .

It can be shown that the spectral radius of the one-step IMEX-RK update matrix corresponding to the 2nd-order 2-stage trapezoidal rule and strong Gauss-Seidel predictor is

$$\rho(\mathbf{C}) = \max \left\{ 1, \left| \frac{1 + \frac{\Delta t \lambda_1}{2} \quad 1 + \frac{\Delta t \lambda_2}{2}}{1 - \frac{\Delta t \lambda_1}{2} \quad 1 - \frac{\Delta t \lambda_2}{2}} \right| \right\}, \quad (\text{A.1})$$

which is independent of  $\alpha$ , less than unity for all  $\Delta t$ , and therefore the scheme is unconditionally stable for all  $\alpha$ . The spectral radius corresponding to the weak Gauss-Seidel scheme is

$$\rho(\mathbf{C}) = \max \left\{ 1, \left| \frac{1 + \frac{\Delta t(\lambda_1 + \lambda_2)}{2}(1 + \alpha) + \frac{\Delta t^2 \lambda_1 \lambda_2}{4}(1 + \alpha)^2 + \frac{\Delta t^2(\lambda_1^2 + \lambda_2^2)}{2}\alpha + \frac{\Delta t^3 \lambda_1 \lambda_2 (\lambda_1 + \lambda_2)}{4}\alpha^2}{(1 - (1 - \alpha)\frac{\Delta t \lambda_1}{2})(1 - (1 - \alpha)\frac{\Delta t \lambda_2}{2})} \right| \right\}, \quad (\text{A.2})$$

which is unconditionally stable if and only if  $\alpha = 0$ . Finally, the spectral radius corresponding to the strong Jacobi scheme is

$$\rho(\mathbf{C}) = \max \left\{ 1, \left| \frac{(1 + \frac{\Delta t \lambda_1}{2})(1 + \frac{\Delta t \lambda_1}{2}) - \frac{\Delta t^3}{4}(\lambda_1^2 \lambda_2 + \lambda_2^2 \lambda_1)}{(1 - \frac{\Delta t \lambda_2}{2})(1 - \frac{\Delta t \lambda_2}{2})} \right| \right\}, \quad (\text{A.3})$$

which is not unconditionally stable.

For 3rd order 4-stage ARK3(2)4L[2]SA and 4th order 6-stage ARK4(3)6L[2]SA in [19], we consider only the strong Gauss-Seidel predictor. The spectral radius of the update matrices for the third and fourth order schemes are

$$\rho(\mathbf{C}_3) = \max \left\{ 1, \left| \frac{p(\lambda_1 \Delta t, \lambda_2 \Delta t)}{q(\lambda_1 \Delta t, \lambda_2 \Delta t)} \right| \right\}, \quad \rho(\mathbf{C}_4) = \max \left\{ 1, \left| \frac{\bar{p}(\lambda_1 \Delta t, \lambda_2 \Delta t)}{\bar{q}(\lambda_1 \Delta t, \lambda_2 \Delta t)} \right| \right\}, \quad (\text{A.4})$$

respectively, where  $p$  and  $q$  are 6th order polynomials and  $\bar{p}$  and  $\bar{q}$  are 10th order polynomials

$$\begin{aligned}
p(x_1, x_2) &= \sum_{i,j=0}^3 p_{ij} x_1^i x_2^j \\
q(x_1, x_2) &= (1 - ax_1)^3 (1 - ax_2)^3 \\
\bar{p}(x_1, x_2) &= \sum_{i,j=0}^5 \bar{p}_{ij} x_1^i x_2^j \\
\bar{q}(x_1, x_2) &= (1 - \bar{a}x_1)^5 (1 - \bar{a}x_2)^5
\end{aligned} \tag{A.5}$$

and  $a = 0.4358665216$  and  $\bar{a} = 0.25$  are the coefficients of the second entry on the diagonal of the implicit Runge-Kutta Butcher tableau for the ARK3(2)4L[2]SA and ARK4(3)6L[2]SA schemes, respectively. From the coefficients of  $p$  and  $\bar{p}$  in Table A.4 and Table A.5, we observe that

$$|p_{ij}| \leq (-1)^{i+j} q_{ij}, \tag{A.6}$$

which implies the Gauss-Seidel predictors lead to unconditionally stable schemes when  $\lambda_1 \leq 0$  and  $\lambda_2 \leq 0$ .

	0	1	2	3
0	1	-0.307599564300000	-0.237660691030414	0
1	-0.307599564300000	0.0946174918786356	0.0731043252393467	0
2	-0.237660691030414	0.0731043252393467	0	-0.0138993203184737
3	0	0	-0.0138993202982233	0.00685679356380471

Table A.4: Coefficients of  $p_{ij}$

	0	1	2	3	4	5
0	1.0	-0.25	-0.125	0.0104166666865151	0.00911458332517619	0.0
1	-0.25	0.06245	0.03125	-0.00260416668514596	-0.00407734171291718	0.0
2	-0.125	0.03125	0.015625	0.00606937261393480	-0.00389797283406001	1.71399137262393e-4
3	0.0104166666865151	-0.00260416668792851	0.00606937262572686	-0.00535453941337523	0.00164424787309041	-8.30991742855789e-5
4	0.00911458332517619	-0.00407734171177262	-0.00389797283635686	0.00164424787343589	-8.99044034172063e-5	7.55399650866135e-6
5	0.0	0.0	1.71399137131092e-4	-8.30991742950535e-5	7.55399650329534e-6	9.53674314457072e-7

Table A.5: Coefficients of  $\bar{p}_{ij}$

Finally, we consider a more general linear system of ODEs

$$\frac{d\mathbf{u}}{dt} = \mathcal{A}\mathbf{u}, \tag{A.7}$$

where  $\mathcal{A} = \mathcal{L} + \mathcal{D} + \mathcal{U}$  is an  $n \times n$  matrix,  $\mathcal{L}$  is the lower triangular part of  $\mathcal{A}$ ,  $\mathcal{U}$  is the upper triangular part of  $\mathcal{A}$ , and  $\mathcal{D}$  is the diagonal of  $\mathcal{A}$ . In the remainder of this section, we show that if  $\mathcal{A}$  is diagonally dominant with negative diagonal entries and the coupling term is taken as  $\mathbf{c}(\mathbf{u}) = (\mathcal{L} + \mathcal{U})\mathbf{u}$ , both the Jacobi and Gauss-Seidel predictors are unconditionally stable for the forward-backward Euler IMEX scheme (Eq. (41)). The update matrix for the weak/strong Jacobi predictor takes the form

$$\mathbf{C}^J = (\mathcal{I} - \Delta t \mathcal{D})^{-1} (\mathcal{I} + \Delta t \mathcal{U} + \Delta t \mathcal{L}) \tag{A.8}$$

and its spectral radius is

$$\rho(\mathbf{C}^J) \leq \|\mathbf{C}^J\|_\infty = \max_i \frac{\sum_{j \neq i} |\Delta t a_{i,j}| + 1}{1 - \Delta t a_{i,i}} \leq 1, \tag{A.9}$$

where the first inequality follows from the Gershgorin circle theorem and the last uses the assumption of diagonal dominance and negative diagonal entries. This confirms that, under the stated assumptions, the

weak/strong Jacobi predictor with the IMEX1 scheme is unconditionally stable. The update matrix for the weak/strong Gauss-Seidel predictor takes the form

$$\mathbf{C}^{GS} = (\mathcal{I} - \Delta t \mathcal{L} - \Delta t \mathcal{D})^{-1} (\mathcal{I} + \Delta t \mathcal{U}). \quad (\text{A.10})$$

Any of its eigenpairs  $(\lambda, \mathbf{x})$  satisfy the relation

$$(\mathcal{I} - \Delta t \mathcal{L} - \Delta t \mathcal{D})^{-1} (\mathcal{I} + \Delta t \mathcal{U}) \mathbf{x} = \lambda \mathbf{x}, \quad (\text{A.11})$$

which can be re-arranged as

$$(\mathcal{I} + \Delta t \mathcal{U}) \mathbf{x} = (\mathcal{I} - \Delta t \mathcal{L} - \Delta t \mathcal{D}) \lambda \mathbf{x} \quad (\text{A.12})$$

or written as components as

$$x_i + \Delta t \sum_{j>i} a_{ij} x_j + \Delta t \lambda \sum_{j<i} a_{ij} x_j = \lambda x_i - \Delta t \lambda a_{ii} x_i \quad (\text{A.13})$$

for  $i = 1, \dots, N$ . Application of the triangular inequality and division by  $|x_i|$  leads to the relation

$$1 + \Delta t \sum_{j>i} |a_{ij}| \frac{|x_j|}{|x_i|} + \Delta t |\lambda| \sum_{j<i} |a_{ij}| \frac{|x_j|}{|x_i|} = |\lambda| |1 - \Delta t a_{ii}|. \quad (\text{A.14})$$

The assumption of diagonal dominance and negative diagonal entries leads to the following bound

$$|\lambda| |1 - \Delta t a_{ii}| = |\lambda| (1 + \Delta t |a_{ii}|) \geq |\lambda| (1 + \Delta t \sum_{j \neq i} |a_{ij}|). \quad (\text{A.15})$$

On the other hand, if  $i = \arg \max_{1 \leq j \leq n} |x_j|$ , (A.14) leads to

$$|\lambda| |1 - \Delta t a_{ii}| \leq 1 + \Delta t \sum_{j>i} |a_{ij}| + \Delta t |\lambda| \sum_{j<i} |a_{ij}|. \quad (\text{A.16})$$

Combining (A.15) and (A.16), we arrive at

$$|\lambda| (1 + \Delta t \sum_{j>i} |a_{ij}|) \leq 1 + \Delta t \sum_{j>i} |a_{ij}| \quad (\text{A.17})$$

for  $i = \arg \max_{1 \leq j \leq n} |x_j|$ , which leads to the desired result

$$\rho(\mathbf{C}^{GS}) \leq 1 \quad (\text{A.18})$$

and confirms that, under the stated assumptions, the weak/strong Gauss-Seidel predictor with the IMEX1 scheme is unconditionally stable.

## References

- [1] X. Chen, G.-C. Zha, and M.-T. Yang. Numerical simulation of 3-d wing flutter with fully coupled fluid–structural interaction. *Computers & Fluids*, 36(5):856–867, 2007.
- [2] B. Griffith, R. Hornung, D. McQueen, and C. Peskin. An adaptive, formally second order accurate version of the immersed boundary method. *Journal of Computational Physics*, 223(1):10–49, 2007.
- [3] M. Day and J. Bell. Numerical simulation of laminar reacting flows with complex chemistry. *Combustion Theory and Modelling*, 4(4):535–556, 2000.

- [4] D. Gaston, C. Newman, G. Hansen, and D. Lebrun-Grandie. MOOSE: A parallel computational framework for coupled systems of nonlinear equations. *Nuclear Engineering and Design*, 239(10):1768–1778, 2009.
- [5] V. Carstens, R. Kemme, and S. Schmitt. Coupled simulation of flow-structure interaction in turbomachinery. *Aerospace Science and Technology*, 7(4):298–306, 2003.
- [6] G. Tóth. The  $\nabla \cdot B = 0$  constraint in shock-capturing magnetohydrodynamics codes. *Journal of Computational Physics*, 161(2):605–652, 2000.
- [7] B. Hübner, E. Walhorn, and D. Dinkler. A monolithic approach to fluid–structure interaction using space–time finite elements. *Computer Methods in Applied Mechanics and Engineering*, 193(23):2087–2104, 2004.
- [8] C. Michler, S. Hulshoff, E. Van Brummelen, and R. De Borst. A monolithic approach to fluid–structure interaction. *Computers & Fluids*, 33(5):839–848, 2004.
- [9] J. Hron and S. Turek. A monolithic FEM/multigrid solver for an ALE formulation of fluid-structure interaction with applications in biomechanics. *Fluid-Structure Interaction*, pages 146–170, 2006.
- [10] C. Farhat and M. Lesoinne. Two efficient staggered algorithms for the serial and parallel solution of three-dimensional nonlinear transient aeroelastic problems. *Computer Methods in Applied Mechanics and Engineering*, 182(3):499–515, 2000.
- [11] S. Piperno and C. Farhat. Partitioned procedures for the transient solution of coupled aeroelastic problems—Part II: energy transfer analysis and three-dimensional applications. *Computer Methods in Applied Mechanics and Engineering*, 190(24):3147–3170, 2001.
- [12] S. Badia, F. Nobile, and C. Vergara. Fluid–structure partitioned procedures based on Robin transmission conditions. *Journal of Computational Physics*, 227(14):7027–7051, 2008.
- [13] P. Causin, J.-F. Gerbeau, and F. Nobile. Added-mass effect in the design of partitioned algorithms for fluid–structure problems. *Computer Methods in Applied Mechanics and Engineering*, 194(42):4506–4527, 2005.
- [14] X. Zhong. Additive semi-implicit Runge–Kutta methods for computing high-speed nonequilibrium reactive flows. *Journal of Computational Physics*, 128(1):19–31, 1996.
- [15] U. Ascher, S. Ruuth, and R. Spiteri. Implicit-explicit Runge-Kutta methods for time-dependent partial differential equations. *Applied Numerical Mathematics*, 25(2-3):151–167, 1997.
- [16] A. Van Zuijlen, A. de Boer, and H. Bijl. Higher-order time integration through smooth mesh deformation for 3D fluid–structure interaction simulations. *Journal of Computational Physics*, 224(1):414–430, 2007.
- [17] B. Froehle and P.-O. Persson. A high-order discontinuous Galerkin method for fluid–structure interaction with efficient implicit–explicit time stepping. *Journal of Computational Physics*, 272:455–470, 2014.
- [18] E. Cyr, J. Shadid, T. Wildey, E. Phillips, A. Robinson, S. Miller, and R. Pawlowski. Implicit-explicit (IMEX) time integration for multi-physics: Application to ALE and plasma simulation. Technical report, Sandia National Lab.(SNL-NM), Albuquerque, NM (United States), 2016.
- [19] C. Kennedy and M. Carpenter. Additive Runge-Kutta schemes for convection-diffusion-reaction equations. 2001.
- [20] L. Pareschi and G. Russo. Implicit-explicit Runge-Kutta schemes for stiff systems of differential equations. *Recent Trends in Numerical Analysis*, 3:269–289, 2000.

- [21] T. Koto. IMEX Runge–Kutta schemes for reaction–diffusion equations. *Journal of Computational and Applied Mathematics*, 215(1):182–195, 2008.
- [22] T. Tezduyar and Y. Park. Discontinuity-capturing finite element formulations for nonlinear convection-diffusion-reaction equations. *Computer Methods in Applied Mechanics and Engineering*, 59(3):307–325, 1986.
- [23] D. Estep, M. Larson, and R. Williams. *Estimating the error of numerical solutions of systems of reaction-diffusion equations*, volume 696. American Mathematical Soc., 2000.
- [24] D. Estep and R. Freund. Using Krylov-subspace iterations in discontinuous Galerkin methods for nonlinear reaction-diffusion systems. In *Discontinuous Galerkin Methods*, pages 327–335. Springer, 2000.
- [25] P. Roe. Approximate Riemann solvers, parameter vectors, and difference schemes. *Journal of Computational Physics*, 43(2):357–372, 1981.
- [26] J. Peraire and P.-O. Persson. The compact discontinuous galerkin (CDG) method for elliptic problems. *SIAM Journal on Scientific Computing*, 30(4):1806–1824, 2008.
- [27] C. Farhat, M. Lesoinne, and N. Maman. Mixed explicit/implicit time integration of coupled aeroelastic problems: Three-field formulation, geometric conservation and distributed solution. *International Journal for Numerical Methods in Fluids*, 21(10):807–835, 1995.
- [28] C. Farhat, C. Degand, B. Koobus, and M. Lesoinne. Torsional springs for two-dimensional dynamic unstructured fluid meshes. *Computer Methods in Applied Mechanics and Engineering*, 163(1-4):231–245, 1998.
- [29] P.-O. Persson, J. Bonet, and J. Peraire. Discontinuous Galerkin solution of the Navier–Stokes equations on deformable domains. *Computer Methods in Applied Mechanics and Engineering*, 198(17-20):1585–1595, 2009.
- [30] M. J. Zahr and P.-O. Persson. An adjoint method for a high-order discretization of deforming domain conservation laws for optimization of flow problems. *Journal of Computational Physics*, 326:516–543, 2016.
- [31] T. Rendall and C. Allen. Unified fluid–structure interpolation and mesh motion using radial basis functions. *International Journal for Numerical Methods in Engineering*, 74(10):1519–1559, 2008.
- [32] Z. Peng and Q. Zhu. Energy harvesting through flow-induced oscillations of a foil. *Physics of Fluids*, 21(12):123602, 2009.
- [33] C.-K. Lin. On the incompressible limit of the compressible Navier-Stokes equations. *Communications in Partial Differential Equations*, 20(3-4):677–707, 1995.
- [34] B. Desjardins, E. Grenier, P.-L. Lions, and N. Masmoudi. Incompressible limit for solutions of the isentropic Navier–Stokes equations with Dirichlet boundary conditions. *Journal de Mathématiques Pures et Appliquées*, 78(5):461–471, 1999.
- [35] C. Kleinstreuer and Z. Zhang. Laminar-to-turbulent fluid-particle flows in a human airway model. *International Journal of Multiphase Flow*, 29(2):271–289, 2003.
- [36] G. Jacobs and J. Hesthaven. Implicit–explicit time integration of a high-order particle-in-cell method with hyperbolic divergence cleaning. *Computer Physics Communications*, 180(10):1760–1767, 2009.
- [37] A. Ferrante and S. Elghobashi. On the physical mechanisms of two-way coupling in particle-laden isotropic turbulence. *Physics of Fluids*, 15(2):315–329, 2003.